Structure-Based Optimization of Small-Molecule Inhibitors for the #-Catenin/B-Cell Lymphoma 9 Protein–Protein Interaction

Min Zhang, Zhen Wang, Yongqiang Zhang, Wenxing Guo, and Haitao Ji

J. Med. Chem., **Just Accepted Manuscript** • DOI: 10.1021/acs.jmedchem.8b00068 • Publication Date (Web): 22 Mar 2018

Structure-Based Optimization of Small-Molecule Inhibitors for the β-Catenin/B-Cell Lymphoma 9 Protein–Protein Interaction

Min Zhang,[†] *Zhen Wang,*[†] *Yongqiang Zhang,*[‡] *Wenxing Guo,*[§] *Haitao Ji**

Drug Discovery Department, H. Lee Moffitt Cancer Center and Research Institute, Tampa, Florida, USA.

Departments of Oncologic Sciences and Chemistry, University of South Florida, Tampa, Florida, USA

The present addresses:

[†] These two authors contribute equally to this work.

[‡] Shanghai Key Laboratory of New Drug Design, School of Pharmacy, State Key Laboratory of Bioengineering Reactor, East China University of Science and Technology, Shanghai, 200237, China.

[§] The Graduate Program, Department of Chemistry, University of Utah, Salt Lake City, Utah, 84112, USA.

*** To whom correspondence should be addressed:**

Haitao Ji, Ph.D.

Drug Discovery Department, H. Lee Moffitt Cancer Center and Research Institute, 12902 Magnolia Drive, MRC room 4047, Tampa, Florida 33612–9416, USA

Phone: 813-745-8070

Fax: 813-745-4506

E-mail: Haitao.Ji@moffitt.org

Keywords: Structure-based drug design, *β*-Catenin, B-cell lymphoma 9, Protein–protein interaction, Inhibitors, Selectivity, Wnt signaling, Synthesis.

Running title: Structure-based optimization of *β*-catenin/BCL9 inhibitors

ABSTRACT

Structure-based optimization was conducted to improve the potency, selectivity, and cell-based activities of *β*-catenin/B-cell lymphoma 9 (BCL9) inhibitors based on the 4'-fluoro-*N*-phenyl-[1,1'-biphenyl]-3-carboxamide scaffold, which was designed to mimic the side chains of the hydrophobic *α*-helical hot spots at positions *i*, *i* + 3, and *i* + 7. Compound **29** was found to disrupt the *β*-catenin/BCL9 protein–protein interaction (PPI) with a K_i of 0.47 μM and >1900-fold selectivity for *β*-catenin/BCL9 over *β*-catenin/E-cadherin PPIs. The proposed binding mode of new inhibitors was consistent with the results of site-directed mutagenesis and structure-activity relationship studies. Cell-based studies indicated that **29** disrupted the *β*-catenin/BCL9 interaction without affecting the *β*-catenin/E-cadherin interaction, selectively suppressed transactivation of Wnt/*β*-catenin signaling, downregulated expression of Wnt target genes, and inhibited viability of Wnt/*β*-catenin dependent cancer cells in dose-dependent manners. A comparison of the biochemical and cell-based assay results offered the directions for future inhibitor optimization.

INTRODUCTION

The Wnt/*β*-catenin signaling pathway plays a key role in directing cell proliferation, differentiation, and survival.[1,2] *β*-Catenin is the central mediator of this signaling pathway. The loss-of-function mutations in the suppressor genes of the Wnt/*β*-catenin signaling pathway, such as adenomatous polyposis coli (*APC*) and *Axin*, and/or the activation mutations at the *N*-terminal phosphorylation sites of the *β*-catenin gene (*CTNNB1*), stabilize *β*-catenin into the dephosphorylated state and result in accumulation of *β*-catenin in the cytoplasm. *β*-Catenin is then translocated into the cell nucleus, where it displaces the repressor protein Groucho/TLE, binds with the T-cell factor (Tcf)/lymphoid enhancer-binding factor (Lef) family of transcription factors, and recruits co-activators, B-cell lymphoma 9 (BCL9), Pygo, CREB-binding protein (CBP), etc. to activate transcription of specific Wnt/*β*-catenin target genes, such as *cyclin D1*, *c-myc*, *survivin*, and *LEF1*. These Wnt target genes then cause the initiation and progression of cancers[3–6] and fibroses[7–9]. The other causes for the hyperactivation of Wnt/*β*-catenin signaling are the autocrine/paracrine activation of Wnt ligands, frizzled (Fzd), and dishevelled (Dvl), and the epigenetic silencing of Wnt antagonist genes. Wnt/*β*-catenin signaling is also hyperactive in cancer stem cells to maintain the self-renewal of cancer stem cells,[10–14] seed cancer metastasis,[15] and drive the resistance to the current therapies[16–19]. On the other hand, tumor cell intrinsic activation of *β*-catenin signaling prevents the recruitment of $CD103^+$ dendritic cells by suppression of chemokine CCL4 expression and excludes $CD8^+$ T-cells from the tumor microenvironment.[20,21] The activation of *β*-catenin signaling was also reported to promote intratumoral regulator T cell (Treg) survival and infiltration, suppressing T-cell immunity.[22,23]

Significant efforts have been made to discover inhibitors for the upstream effectors of the Wnt/*β*-catenin signaling pathway.[24–31] However, the inhibition of the upstream Wnt effectors can

potentially cause the cross-regulatory effects on the noncanonical Wnt signaling pathways. Second, these inhibitors cannot confer efficacy to the diseases that harbor the more downstream *APC* and *Axin* loss-of-function mutations and the *β*-catenin activation mutations. The formation of the *β*-catenin-containing transcriptional complex in the cell nucleus is the penultimate step of this pathway. The transcriptional overactivation of Wnt/*β*-catenin signaling is dependent on the formation of this complex, in which *β*-catenin interacts with BCL9.[32] BCL9 functions as a scaffolding structure of the Wnt enhanceosome and brings *β*-catenin to Tcf/Lef to transcribe specific Wnt target genes that cause the diseases.[33] The crystallographic analysis[34,35] and the biochemical studies[36–38] reveal that the homology domain 2 (HD2) of BCL9/B9L adopts an *α*-helical structure to interact with the first armadillo repeat of *β*-catenin. Mammalian genomes encode two BCL9 paralogues, BCL9 and B9L (BCL9-like).[39,40] The use of siRNAs[39–42] and shRNAs[43] against *BCL9*/*B9L* markedly decreases *β*-catenin-dependent gene expression and diminishes the growth of cancer cells *in vitro* and *in vivo*. The dominant negative constructs of BCL9/B9L that lack the *C*-terminal domains greatly inhibit the activity of Wnt/*β*-catenin signaling.[39,41] Hence, the inhibitors that can disrupt the *β*-catenin/BCL9 protein–protein interaction (PPI) not only provide new chemical probes to understand the biology regulated by *β*-catenin signaling, but also offer the important starting points for drug discovery to treat advanced cancers and fibroses.

Triazole-stapled[44] and olefin-stapled[45] BCL9 L351–F374 *α*-helical peptides have been reported. The olefin-stapled BCL9 peptide was reported to target *β*-catenin, disrupt the *β*-catenin/BCL9 PPI, and suppress transcription of Wnt target genes. This stapled peptide also inhibited tumor cell growth, angiogenesis, and metastasis without overt damage to normal tissues in mouse xenograft models for colorectal carcinoma and multiple myeloma.[45] Compound

screening identified a small molecule, carnosic acid, that disrupted the *β*-catenin/BCL9 PPI and inhibited *β*-catenin dependent transcription.[35,46] In the previous study, we designed 4'-fluoro-*N*-phenyl-[1,1'-biphenyl]-3-carboxamide as a generalizable scaffold that itself can directly mimic the side chains of *α*-helical hot spots at positions *i*, *i* + 3, and *i* + 7.[47] The further derivatization generated **1** in Figure 1. The biochemical AlphaScreen assay indicated that **1** disrupted the *β*-catenin/BCL9 PPI with an inhibition constant (K_i) of 2.1 ± 0.41 μM and showed 125-fold selectivity for *β*-catenin/BCL9 over *β*-catenin/E-cadherin PPIs.[47] The proposed binding mode of **1** was evaluated with the site-directed mutagenesis studies using *β*-catenin D145A, E155A, D145A/E155A, L159S, and L156S/L178S and the structure-activity relationship (SAR) studies of 29 derivatives. The cellular bioavailability studies indicated that **1** can easily be taken up by cancer cells.[48] This compound also dissociated the *β*-catenin/BCL9 PPI in cells, selectively suppressed transactivation of Wnt/*β*-catenin signaling, downregulated expression of Wnt target genes, and inhibited growth of Wnt/*β*-catenin-dependent cancer cells. To further improve the potency and selectivity of this series of inhibitors, herein, we report the structure-based optimization, synthesis, and biological characterization of new derivatives.

RESULTS

1. Inhibitor Design and Synthesis

(a) Explore the hydrophobic interaction. As described in the previous studies, the *β*-catenin/BCL9 PPI interface has two hot regions.[34,36–38,41,47,49] In hot region 1, residues D162, E163, and D164 of human *β*-catenin form an acidic knob to interact with H358 and R359 of human BCL9.[34,36–38,41] This PPI interface is shallow and dominated by electrostatic interactions. In hot region 2, residues L366 (*i*), I369 (*i* + 3), and L373 (*i* + 7) of human BCL9 interact with a

surface pocket that is lined with L159, V167, A171, M174, L178, L148, A149, A152, and L156 of human *β*-catenin, as shown in Supplementary Figure S1.[34,41,44,47] This PPI interface is dominated by the hydrophobic interaction. The model of the interaction of **1** with *β*-catenin reported in the previous study[47] was used as the starting point for inhibitor optimization. The first step of inhibitor design based on **1** was to increase its hydrophobic interactions with *β*-catenin. Compounds **2**–**8** in Figure 1 were designed and synthesized. The synthetic route for **2** and **3** is shown in Scheme 1. The synthetic route for **4**–**8** is shown in Supplementary Scheme S1. The AlphaScreen assay[50] was used to evaluate the inhibitory activities of **2**–**8** in *in vitro* biochemical assays using full-length *β*-catenin and the BCL9 peptide (G350–P375). The results were expressed as the K_i in Figure 1. Compounds **2** and **3** displayed the similar biochemical activities as **1**, indicating the limited gain of the potency by increasing the hydrophobic interaction.

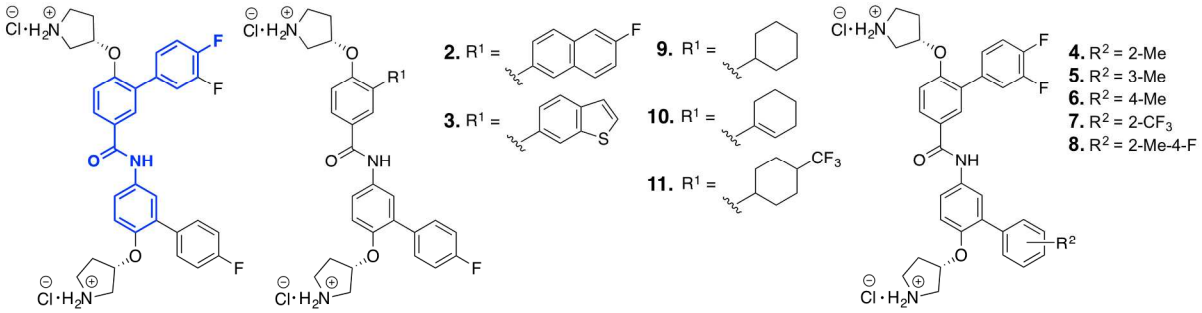

1 **2, 3, 9–11** **4–8**

No.	K_i ± SD (*μ*M) *β*-catenin/BCL9	No.	K_i ± SD (*μ*M) *β*-catenin/BCL9
1	1.5 ± 0.87	**7**	3.8 ± 1.3
2	1.3 ± 0.76	**8**	3.5 ± 1.3
3	1.4 ± 0.76	**9**	14 ± 1.6
4	5.9 ± 1.8	**10**	7.1 ± 2.5
5	3.1 ± 1.3	**11**	4.2 ± 2.3
6	6.5 ± 1.7		

Figure 1. The chemical structures and the AlphaScreen K_i values of **1**–**11**. Each set of data was expressed as mean ± standard deviation (n = 3).

The 3, 4-difluorophenyl ring of **1** was also replaced with the aliphatic ring to explore the hydrophobic interaction. Compounds **9**–**11** were designed and synthesized. The synthetic route of **9**–**11** is shown in Supplementary Scheme S2. The AlphaScreen assay results in Figure 1 indicated that these three compounds were not as potent as **1**.

(b) Search for the favorable polar interactions. Although the hot region 2 is primarily hydrophobic, it does have the helical dipole and the polar functional groups. One strategy we used was the replacement of the CH group in the aromatic rings of **1** with the N atom.[51] This method introduces the polarity to the compounds and reduces the lipophilicity. Compounds **12**–**16** were designed and synthesized. The synthetic routes for **12** and **13** are shown in Supplementary Scheme S3. The synthetic routes for **14**–**16** are shown in Supplementary Scheme S4. The biochemical assay results of **12**–**16** in Figure 2 indicated none of these compounds were as potent as **1**.

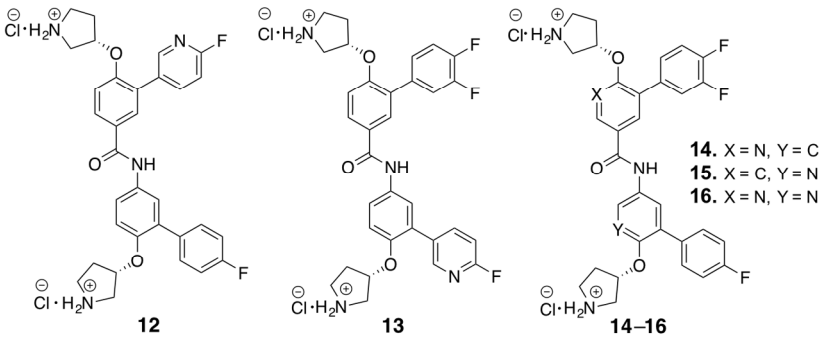

No.	K_i ± SD (μM) β-catenin/BCL9
12	19 ± 3.8
13	16 ± 3.4
14	8.7 ± 4.1
15	8.2 ± 2.4
16	7.3 ± 1.8

Figure 2. The chemical structures and the AlphaScreen K_i values of **12**–**16**. Each set of data was expressed as mean ± standard deviation (n = 3).

(c) Search for the favorable H-bonding and salt bridge interactions. The crystal structures of *β*-catenin in complex with the BCL9 HD2 domain shows *β*-catenin Lys181 is adjacent to the hot region 2.[34,35] Another strategy for inhibitor optimization was targeting this residue. Compounds **17**–**23** were designed to form H-bonding interactions with *β*-catenin Lys181. The synthetic route for **17**–**23** is shown in Supplementary Scheme S5. Carboxylic acid and bioisosteres were introduced to **1** to form salt bridge interactions with Lys181. Compounds **24**–**30** were designed and synthesized. The synthetic route for **24**–**26** is shown in Supplementary Scheme S6. The synthetic routes for **27**–**30** are shown in Scheme 2. The AlphaScreen assay results of **17**–**30** are shown in Figure 3. The biochemical inhibitory activities of **27** and **30** were comparable with that of **1**. Compound **29** exhibited the K_i of 0.47 ± 0.14 μM for disruption of the *β*-catenin/BCL9 PPI. This K_i value is very close to the dissociation constant (K_D) of 0.47 μM for the *β*-catenin/BCL9 interaction.[34]

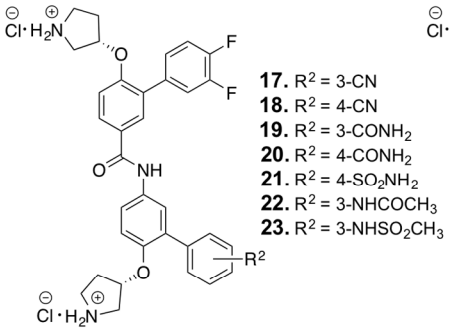

17. R^2 = 3-CN
18. R^2 = 4-CN
19. R^2 = 3-$CONH_2$
20. R^2 = 4-$CONH_2$
21. R^2 = 4-SO_2NH_2
22. R^2 = 3-$NHCOCH_3$
23. R^2 = 3-$NHSO_2CH_3$

17–23

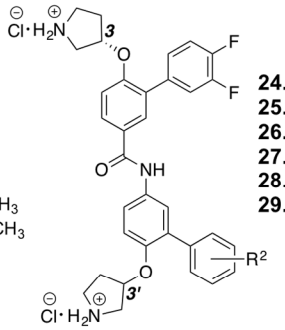

24. 3*S*, 3'*S*, R^2 = 3-CO_2H
25. 3*S*, 3'*S*, R^2 = 2-F, 5-CO_2H
26. 3*S*, 3'*S*, R^2 = 4-CO_2H
27. 3*S*, 3'*S*, R^2 = 3-tetrazole
28. 3*S*, 3'*S*, R^2 = 4-tetrazole
29. 3*S*, 3'*R*, R^2 = 3-tetrazole

24–29

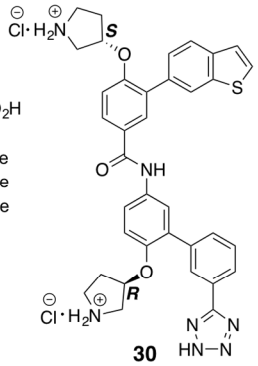

30

No.	K_i ± SD (μM) *β*-catenin/BCL9	No.	K_i ± SD (μM) *β*-catenin/BCL9	No.	K_i ± SD (μM) *β*-catenin/BCL9
17	4.2 ± 2.0	**22**	5.2 ± 2.2	**27**	1.6 ± 0.78
18	3.8 ± 2.1	**23**	5.9 ± 3.0	**28**	4.6 ± 2.0
19	5.6 ± 2.5	**24**	5.4 ± 2.3	**29**	0.47 ± 0.14
20	4.7 ± 2.9	**25**	12 ± 2.3	**30**	1.6 ± 0.23
21	5.6 ± 2.2	**26**	3.7 ± 1.9		

Figure 3. The chemical structures and the AlphaScreen K_i values of **17**–**30**. Each set of data was expressed as mean ± standard deviation (n = 3).

(d) Introduce conformational constraints. Two compounds, **31** and **32**, were designed and synthesized. The synthetic routes for **31** and **32** are shown in Scheme 3. The biochemical assay results of these two compounds are shown in Figure 4. Compound **32** exhibited the similar biochemical inhibitory activity as **1**.

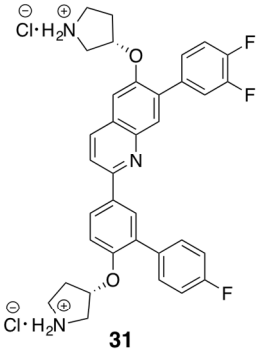

31

No.	K_i ± SD (μM) β-catenin/BCL9
31	8.0 ± 1.8

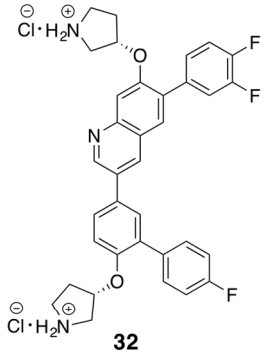

32

No.	K_i ± SD (μM) β-catenin/BCL9
32	2.2 ± 0.84

Figure 4. The chemical structures and the AlphaScreen K_i values of **31** and **32**. Each set of data was expressed as mean ± standard deviation (n = 3).

2. Biochemical Characterizations.

(a) Inhibitor selectivity between *β*-catenin/BCL9 and *β*-catenin/E-cadherin PPIs. *β*-Catenin is at least associated with two functions in cells. One is that the nuclear *β*-catenin interacts with Tcf/Lef, BCL9/B9L, CBP/p300, etc. to culminate Wnt/*β*-catenin signaling. The second is that the cytosolic *β*-catenin interacts with E-cadherin to act as a structural component of adherens junctions. The crystallographic analyses of *β*-catenin in complexes with BCL9[34,35] and E-

cadherin[52] indicated that the interface of β-catenin to interact with BCL9 was also used to bind region V of E-cadherin. Compounds **29** and **30** were assessed for their selectivity between β-catenin/BCL9 and β-catenin/E-cadherin PPIs using the AlphaScreen selectivity assay.[50] As shown in Table 1, these two compounds exhibited high selectivity for β-catenin/BCL9 over β-catenin/E-cadherin PPIs with **29** of >1900-fold.

Table 1. The selectivities of **29** and **30** between β-catenin/BCL9 over β-catenin/E-cadherin interactions. Each set of data was expressed as mean ± standard deviation (n = 3).

	K_i ± SD (μM)		Selectivity
Compounds	β-catenin/BCL9	β-catenin/E-cadherin	BCL9/cadherin
29	0.47 ± 0.14	>915	>1900
30	1.6 ± 0.23	>915	>570

(b) Site-directed mutagenesis studies. In the previous studies, compound **1** was reported to bind with β-catenin but not the BCL9 HD2 domain in isothermal titration calorimetry (ITC) studies.[47] The crystallographic studies indicated that D145, E155, and K181 were not involved in the β-catenin/BCL9 binding.[34,35] Our AlphaScreen and fluorescence polarization (FP) experiments indicated that β-catenin D145A,[47] E155A,[47] D145A/E155A,[47] and K181A mutants had no effect on the β-catenin/BCL9 PPI, as shown in Figure 5A. This result allowed us to use the AlphaScreen competitive inhibition assays to evaluate the effects of these mutations on the K_i of **3**, **27**, and **29**. As shown in Figure 5B, the K_i values of **3** for wild type β-catenin/BCL9, β-catenin D145A/BCL9, and β-catenin D145A and E155A/BCL9 interactions were 1.3 ± 0.80, 4.2 ± 1.1 and 12 ± 3.8 μM, respectively, indicating that the carboxylic side chains of both D145 and

E155 of β-catenin were important for the inhibitory potency of **3**. However, β-catenin K181 was not targeted by **3**, because the K_i value of **3** for the β-catenin K181A/BCL9 interaction was 1.7 ± 0.26 μM. This result is consistent with the proposed binding mode of **3** with β-catenin in Figure 5C (The stick models of Figure 5C is shown in Supplementary Figure S2A). Compounds **27** and **29** were designed to form salt bridge interactions with β-catenin K181A. The AlphaScreen K_i of these two compounds for wild type β-catenin/BCL9, β-catenin D145A/BCL9, β-catenin D145A and E155A/BCL9, and β-catenin K181A/BCL9 PPIs are shown in Figure 5B. β-Catenin D145, E155, and K181 are important for **27** and **29** to bind with β-catenin and disrupt the β-catenin/BCL9 PPI. This result is consistent with the proposed binding mode in Figure 5D (The stick models of Figure 5D is shown in Supplementary Figure S2B).

A

β-catenin	apparent K_D ± SD (μM) AlphaScreen	FP
wild type	0.71 ± 0.079	0.74 ± 0.099
D145A	0.65 ± 0.072	0.76 ± 0.16
E155A	0.76 ± 0.047	0.70 ± 0.074
D145A/E155A	0.86 ± 0.080	0.82 ± 0.11
K181A	0.68 ± 0.021	0.62 ± 0.12

B

β-catenin	K_i ± SD (μM) **3**	**27**	**29**
Wild type	1.3 ± 0.80	1.0 ± 0.34	0.47 ± 0.14
D145A	4.2 ± 1.1	6.5 ± 2.5	3.0 ± 1.0
D145A/ E155A	12 ± 3.8	18 ± 5.7	12 ± 3.3
K181A	1.7 ± 0.26	4.9 ± 1.7	4.1 ± 2.2

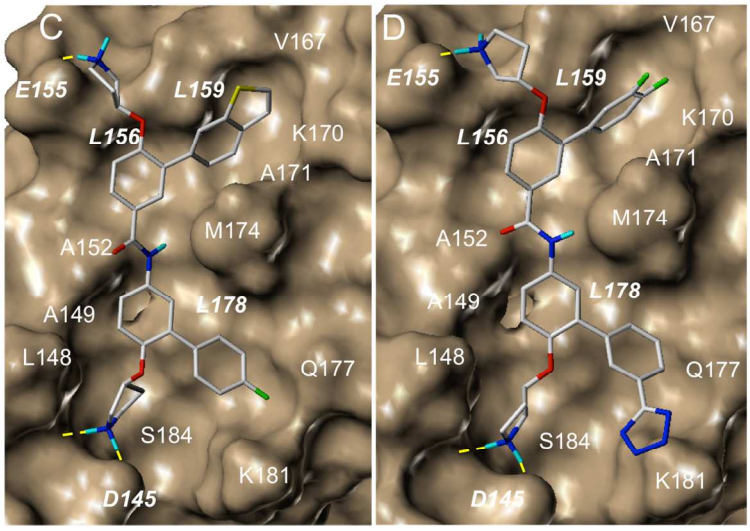

Figure 5. (A) The apparent K_D values of wild-type and mutant β-catenin proteins with wild-type BCL9 HD2 domain. (B) AlphaScreen competitive inhibition assay of **3**, **27**, and **29** to disrupt wild-type β-catenin/wild-type BCL9 and mutant β-catenin/wild-type BCL9 PPIs. Each set of data was expressed as mean ± standard deviation (n = 3). (C) AutoDock docking result of **3** with β-catenin (PDB ID, 2GL7). (D) AutoDock docking result of **29** with β-catenin (PDB ID, 2GL7).

3. Cell-Based Studies.

(a) Inhibition of viability of Wnt/*β*-catenin-dependent cancer cells. The MTS assay was conducted to determine the effects of **1**–**32** on inhibition of cancer cell growth. Three cancer cell lines with hyperactive Wnt/*β*-catenin signaling, SW480, HCT116, and MDA-MB-231, and one cancer cell line with the normal Wnt/*β*-catenin signaling pathway, A549, were used in this study. The tested compounds were incubated with cells for 72 h before the addition of the MTS reagent (3-(4,5-dimethylthiazol-2-yl)-5-(3-carboxymethoxyphenyl)-2-(4-sulfophenyl)-2H-tetrazolium, inner salt) and the electron coupling reagent, phenazine methosulfate (PMS), for detection.[53,54] The half maximal inhibitory concentrations (IC_{50}) of these compounds are shown in Table 2. All of the compounds inhibited viability of cancer cells. Among them, compounds **4**, **8**, **14**, **15**, **27**, **29**, and **31** are selective for Wnt/*β*-catenin hyperactive cancer cells over the cancer cells that have normal Wnt signaling.

(b) Lactate dehydrogenase (LDH) cytotoxicity assay. The cytotoxic compounds may cause cell death by damaging of the cell membrane through the nonspecific manner. The LDH release assay[55,56] with the relatively short inhibitor incubation time[57] (4 h in this study) was conducted to determine the cytotoxicity of the tested compounds. The result is shown in Supplementary Figure S3. Compounds **1**–**18** except **12** exhibited nonspecific cytotoxicity at high concentrations, such as 50 and 100 μM. Compounds **19**–**31** did not exhibit obvious cytotoxicity in the LDH assay even at the very high concentration of 800 μM.

Table 2. The MTS assay to monitor the inhibitory activities of **1**–**32** on viability of cancer cells, and the Wnt-responsive TOPFlash luciferase reporter assay to examine effect on Wnt/*β*-catenin

transactivation. Each set of data was expressed as mean ± standard deviation (n = 3). The data for **1** was reported in the previous study.[47]

	MTs IC_{50} ± SD (μM)				TOPFlash IC_{50} ± SD (μM)	
	Wnt/β-catenin hyperactive			normal Wnt	β-catenin-activated	
No.	SW480	HCT116	MDA-MB-231	A549	HEK239	SW480
1	3.5 ± 0.32	3.1 ± 0.83	2.3 ± 0.25	8.8 ± 0.62	4.5 ± 1.3	2.9 ± 0.33
2	1.8 ± 0.94	5.6 ± 2.2	2.1 ± 1.1	3.7 ± 1.4	10 ± 3.4	12 ± 3.5
3	2.0 ± 0.80	7.5 ± 2.0	2.8 ± 1.7	9.4 ± 3.3	6.2 ± 1.9	1.2 ± 0.27
4	1.2 ± 0.62	5.7 ± 1.9	3.1 ± 1.5	23 ± 5.0		5.2 ± 1.3
5	2.2 ± 1.3	1.4 ± 0.6	1.4 ± 0.7	4.5 ± 2.0		
6	1.6 ± 0.71					
7	2.6 ± 0.67					
8	0.90 ± 0.51	5.6 ± 2.0	4.1 ± 1.8	10 ± 2.4		2.0 ± 0.29
9	6.6 ± 2.7	3.8 ± 1.5		3.8 ± 1.5		
10	3.7 ± 2.0	6.9 ± 3.2	3.4 ± 1.6	8.9 ± 2.7		8.7 ± 2.3
11	3.6 ± 2.7	5.6 ± 2.7	2.3 ± 1.0	4.8 ± 2.4	10 ± 3.2	10 ± 3.3
12	21 ± 8.0					
13	15 ± 4.1					
14	3.0 ± 1.4	8.7 ± 3.5	3.6 ± 1.2	26 ± 7.4	22 ± 4.5	5.9 ± 1.0
15	1.7 ± 0.99	7.8 ± 3.3	3.1 ± 1.3	29 ± 7.9	10 ± 1.2	7.7 ± 1.2
16	9.9 ± 3.7					
17	4.3 ± 0.74				>25	
18	6.1 ± 2.9				>25	
19	190 ± 15					
20	160 ± 19					
21	220 ± 58				>200	>200
22	160 ± 9.1					
23	95 ± 8.9					

24	>400	>400				368 ± 30
25	>400	>400				>400
26	>400	>400				391 ± 36
27	140 ± 11	190 ± 7.8	92 ± 16	410 ± 42		
28	86 ± 13					
29	41 ± 6.2	55 ± 7.4	73 ± 8.9	>400	25 ± 4.1	25 ± 2.7
30	150 ± 21	240 ± 29		430 ± 30	50 ± 5.2	43 ± 3.4
31	3.6 ± 1.9	9.6 ± 2.5	15 ± 6.1	23 ± 4.4	26 ± 3.1	12 ± 1.5
32	1.7 ± 0.90	2.2 ± 1.0	3.1 ± 1.2	7.5 ± 2.9	14 ± 1.5	7.9 ± 1.4

(c) Inhibition of *β*-catenin/BCL9/Tcf transcriptional activity. The TOPFlash luciferase reporter assay (in which the luciferase reporter has three wild-type Tcf4 binding sites) was performed with **1**–**4**, **8**, **10**, **11**, **14**, **15**, **17**, **18**, **21**, and **29**–**32**. Their IC_{50} values are shown in Table 2. Among them, compounds **1**–**4**, **8**, **10**, **11**, **14**, **15**, and **29**–**32** inhibited the TOPFlash luciferase activities. However, all of these compounds, except **29** and **30**, inhibited the FOPFlash luciferase reporter (with three mutant Tcf4 binding sites) activities at the higher concentrations. The results of **1**–**4**, **8**, **11**, **14**, **15**, and **29**–**32** are shown in Figure 6. These results indicated that only **29** and **30** are specific for the Wnt/*β*-catenin signaling pathway. Compounds **1**–**4**, **8**, **11**, **14**, and **15** inhibited FOPFlash luciferase reporter activity because these compounds underwent the primary necrosis by damaging the cell membrane at high concentrations.

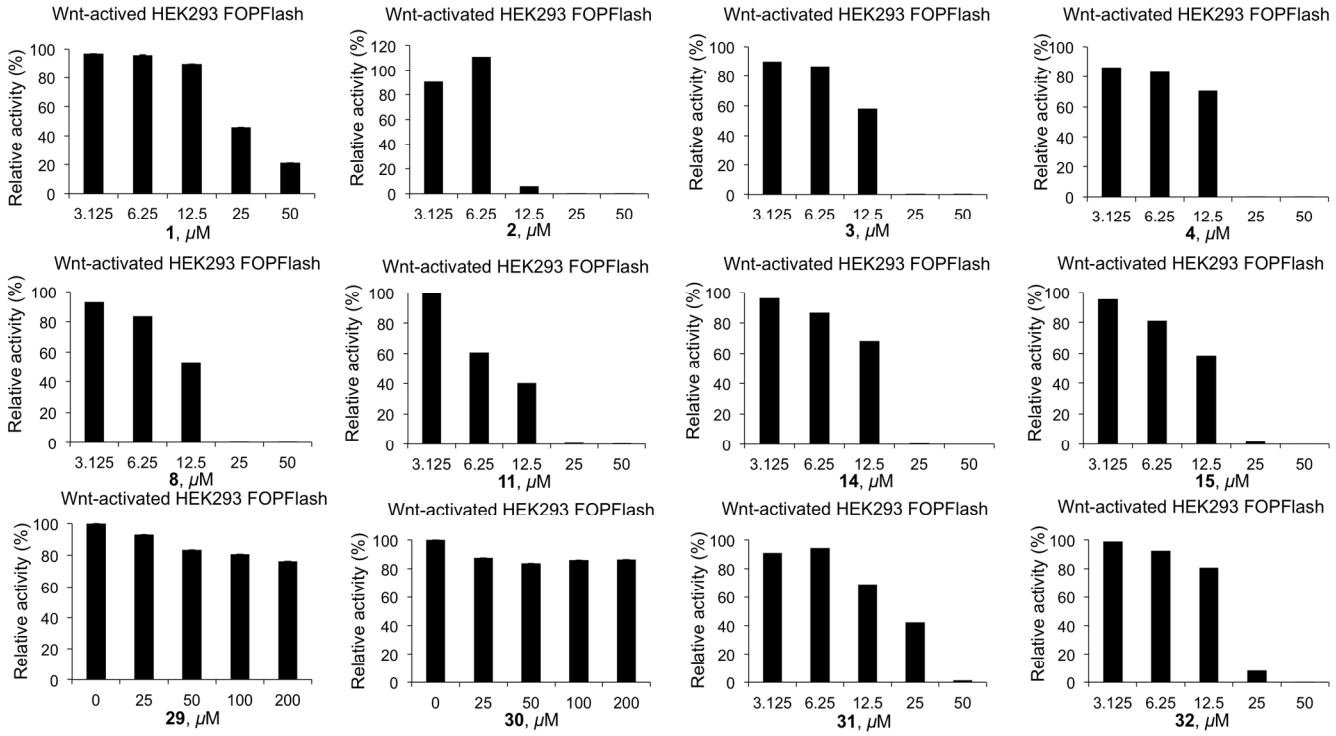

Figure 6. Wnt-responsive FOPFlash luciferase reporter assay results of inhibitors **1**–**4**, **8**, **11**, **14**, **15**, and **29**–**32** in *β*-catenin activated HEK293 cells.

(d) Inhibition of expression of Wnt/*β*-catenin target genes. *Axin2* is a specific target gene of the Wnt/*β*-catenin signaling pathway.[58] *Cyclin D1*, *LEF1*, and *c-myc* are upregulated in cancer cells with hyperactive Wnt/*β*-catenin signaling to promote tumorigenesis. Quantitative real-time PCR (qPCR) studies were conducted for **3**, **8**, **29**, and **31** (Figure 7). Similar to **1**,[47] compounds **3** and **29** did not inhibit house-keeper gene *HPRT*, but dose-dependently inhibited Wnt target genes, *Axin2*, *cyclin D1*, and *LEF1*.

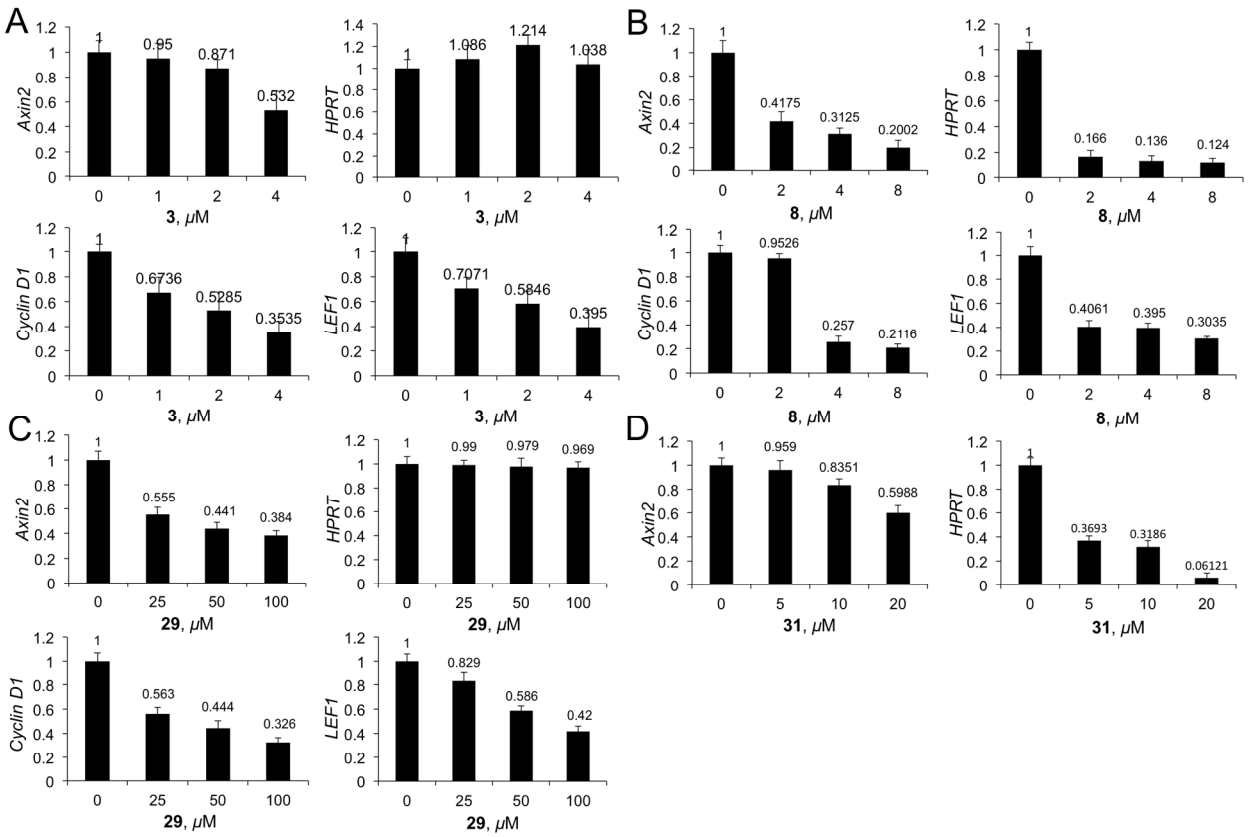

Figure 7. qPCR studies to determine the changes of mRNA expression of *AXIN2*, *LEF1*, and *cyclic D1* in SW480 cells in response to different concentrations of **3** (A), **8** (B), **29** (C), and **31** (D). House-keeper gene *HPRT* was used as the reference. Each set of data was expressed as mean ± standard deviation (n = 3).

As shown in Figure 8A,B, Western blot experiments indicated that the protein expression levels of cyclin D1 and c-myc were significantly decreased after treatment of **3** and **29**, respectively. Both compounds can inhibit the level of the active form of β-catenin (ABC), which is nuclear β-catenin, in dose dependent manners. These two compounds had no effect on the level of E-cadherin-bound β-catenin (i.e., total β-catenin), indicating these two compounds did not affect the upstream nodes of Wnt pathway that regulate degradation of cytosolic β-catenin.

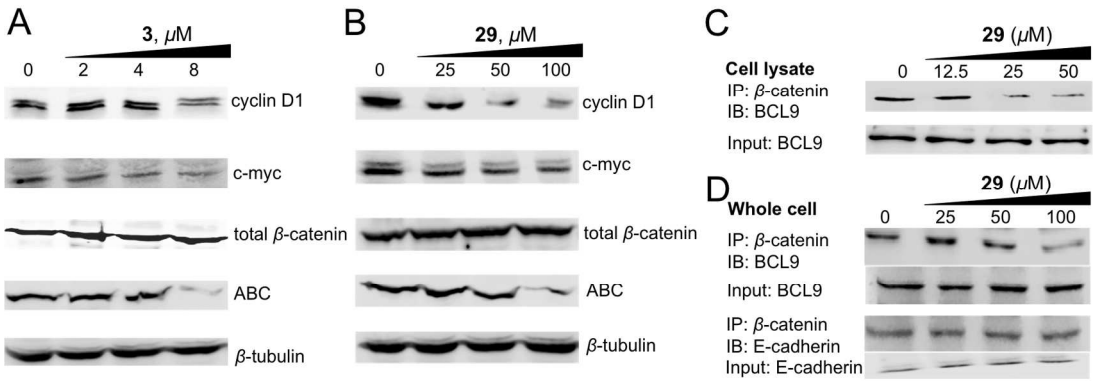

Figure 8. (A and B) Western blot analysis to monitor the change of protein expression of cyclin D1, c-myc, the active form of *β*-catenin (ABC), and the total *β*-catenin in response to different concentrations of **3** (A) and **29** (B) in SW480 cells. *β*-Tubulin was used as the internal reference. The quantitative data of Western blot analyses is shown in Supplementary Table S1 (C) Co-IP experiments to evaluate the disruption of the *β*-catenin/BCL9 PPI by **29** in HCT116 cell lysate. (D) Co-IP experiments to evaluate the disruption of the *β*-catenin/BCL9 PPI by **29** and the selectivity of **29** for *β*-catenin/BCL9 over *β*-catenin/E-cadherin PPIs in HCT116 cells. IP, immunoprecipitation; IB, immunoblotting; input, 10% of cell lysate. Each experiment was performed in triplicate. The quantitative data of co-IP experiments is shown in Supplementary Table S2.

(e) Disruption of the *β*-catenin/BCL9 PPI in cells and cell-based inhibitor selectivity studies. The co-immunoprecipitation (co-IP) experiments were conducted to assess the effect of **29** for disruption of the interaction between full-length *β*-catenin and full-length BCL9 using HCT116 cell lysates. As shown in Figure 8C, compound **29** can dose-dependently disrupt the full-length *β*-catenin/full-length BCL9 PPI after 4 h incubation with HCT116 cell lysates. The co-IP experiments were also performed with HCT116 cells to evaluate the effect of **29** on the disruption of the *β*-catenin/BCL9 PPI and the selectivity over the *β*-catenin/E-cadherin PPI in the

cellular context. As shown in Figure 8D, compound **29** inhibited the *β*-catenin/BCL9 PPI in a dose-dependent manner. A parallel experiment indicated that **29** did not affect the *β*-catenin/E-cadherin PPI at the concentrations that were sufficient to disrupt the *β*-catenin/BCL9 PPI.

4. Chemistry.

The synthetic route for **2** and **3** is shown in Scheme 1. The amide bond coupling reaction between the previously reported **33**[59] and **34**[47] generated key intermediate **35**, which then underwent the Suzuki reaction with (6-fluoronaphthalen-2-yl) boronic acid or (1-benzothiophen-6-yl) boronic acid to afford **36** in good yield. The Boc deprotection of **36** with 4 M HCl offered the final products **2** and **3**.

Scheme 1.

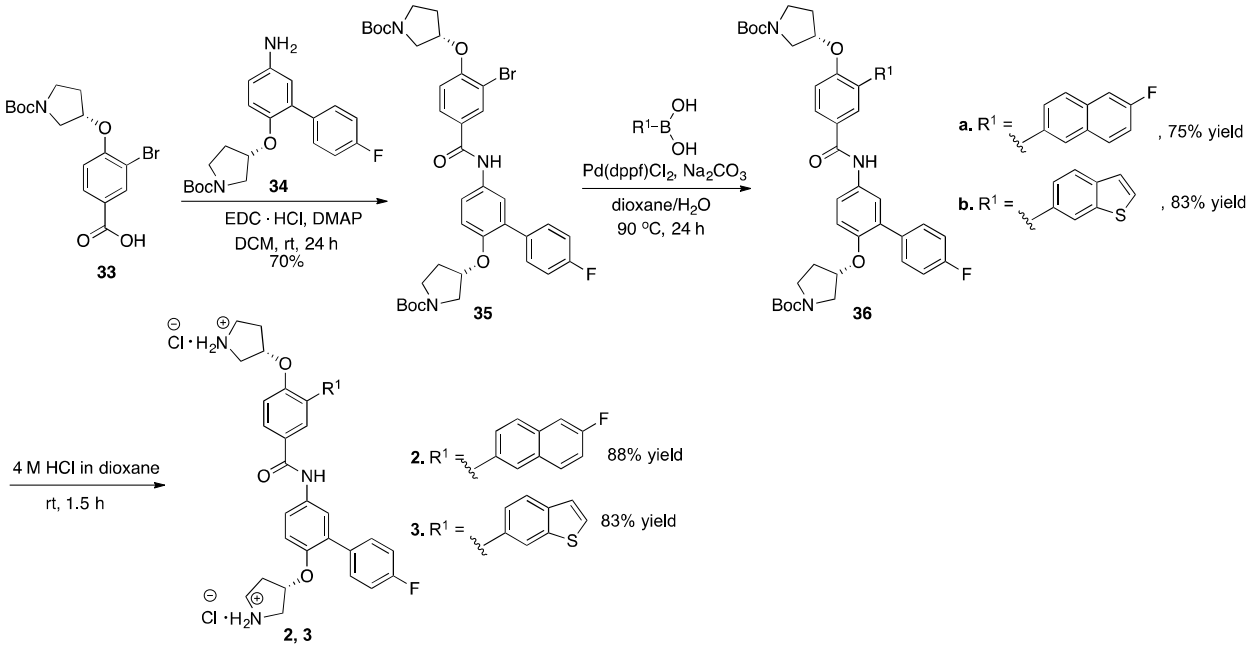

The synthetic routes for **27**–**30** are shown in Scheme 2. Compound **33** was subjected to the Curtius rearrangement to generate **37**. The deprotection of the Cbz protecting group gave **38**. The amide bond coupling reaction of **38** with another previously reported key intermediate **39**[47], and then the Suzuki reaction with 3-cyanophenylboronic acid and 4-cyanophenylboronic acid generated **41a**,**b**, respectively. The cycloaddition reaction of nitriles **41** with *n*-Bu_3SnN_3 and then the deprotection of the Boc protecting group with 4 M HCl offered **27** and **28**. The Suzuki reaction between the previously reported **43**[47] and 3-cyanophenylboronic acid afforded **44**. The hydrolysis of the methyl ester of **44** and the Curtis rearrangement reactions furnished **46**. The deprotection of the Cbz group and the amide bond coupling reaction with **39** gave **48**. The cycloaddition reaction of **48** with *n*-Bu_3SnN_3 resulted in **49**, which offered the final product **29** after the deprotection of the Boc group. The Suzuki reaction between **43** and (1-benzothiophen-6-yl) boronic acid generated **50**. The deprotection of the methyl ester of **50** and the amide coupling reaction with **46** afforded **52**, which then underwent the cycloaddition reaction to furnish **53**. The deprotection of the Boc group of **53** generated final product **30**.

Scheme 2.

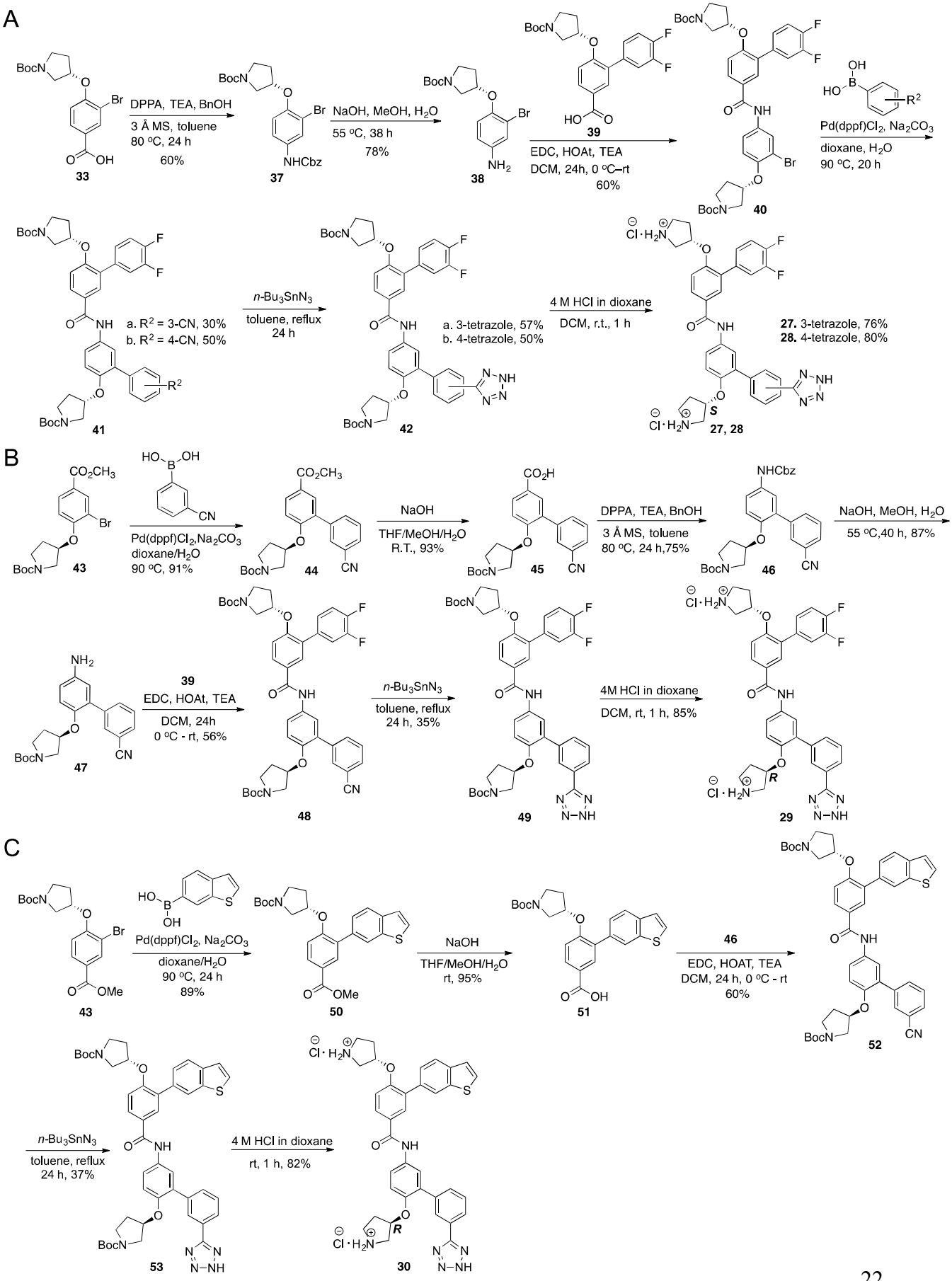
A
DPPA, TEA, BnOH
3 Å MS, toluene
80 °C, 24 h
60%
NaOH, MeOH, H2O
55 °C, 38 h
78%
EDC, HOAt, TEA
DCM, 24h, 0 °C–rt
60%
Pd(dppf)Cl2, Na2CO3
dioxane, H2O
90 °C, 20 h
a. R2 = 3-CN, 30%
b. R2 = 4-CN, 50%
n-Bu3SnN3
toluene, reflux
24 h
a. 3-tetrazole, 57%
b. 4-tetrazole, 50%
4 M HCl in dioxane
DCM, r.t., 1 h
27. 3-tetrazole, 76%
28. 4-tetrazole, 80%
B
Pd(dppf)Cl2,Na2CO3
dioxane/H2O
90 °C, 91%
NaOH
THF/MeOH/H2O
R.T., 93%
DPPA, TEA, BnOH
3 Å MS, toluene
80 °C, 24 h,75%
NaOH, MeOH, H2O
55 °C,40 h, 87%
EDC, HOAt, TEA
DCM, 24h
0 °C - rt, 56%
n-Bu3SnN3
toluene, reflux
24 h, 35%
4M HCl in dioxane
DCM, rt, 1 h, 85%
C
Pd(dppf)Cl2, Na2CO3
dioxane/H2O
90 °C, 24 h
89%
NaOH
THF/MeOH/H2O
rt, 95%
EDC, HOAT, TEA
DCM, 24 h, 0 °C - rt
60%
n-Bu3SnN3
toluene, reflux
24 h, 37%
4 M HCl in dioxane
rt, 1 h, 82%

The synthetic routes for **31** and **32** are shown in Scheme 3. The esterification of 4-bromo-3-hydroxybenzoic acid and then the Mitsunobu reaction with (*R*)-*N*-Boc-3-pyrrolidinol offered **55**. The Suzuki reaction of **55** with 3, 4-difluorophenylboronic acid and the hydrolysis of the methyl ester of **56** afforded **57**. The Curtius rearrangement of **57** and the deprotection of the Cbz group generated **59**. The methyl ester group of the previously synthesized intermediate **60**[47] was reduced to a hydroxymethyl group by DIBAL-H. The alcohol **61** was then oxidized to aldehyde **62** by PCC. The expoxidation of **62** by trimethylsulfoxonium iodide offered **63**. The palladium-catalyzed sequential reaction[60] using the previously reported aniline **64**[47], aldehyde **62**, and acrylic acid produced **65**. The other regioisomer **65a** was not observed in this reaction. This difference might be correlated with the steric hindrance of the 3, 4-difluorophenyl ring. The deprotection of the Boc protecting group afforded the final product **31**. The $FeCl_3$ promoted tandem reaction of aniline **59** with styrene oxide **63** furnished **66**.[61] The deprotection of the Boc protecting group provided the final product **32**.

Scheme 3.

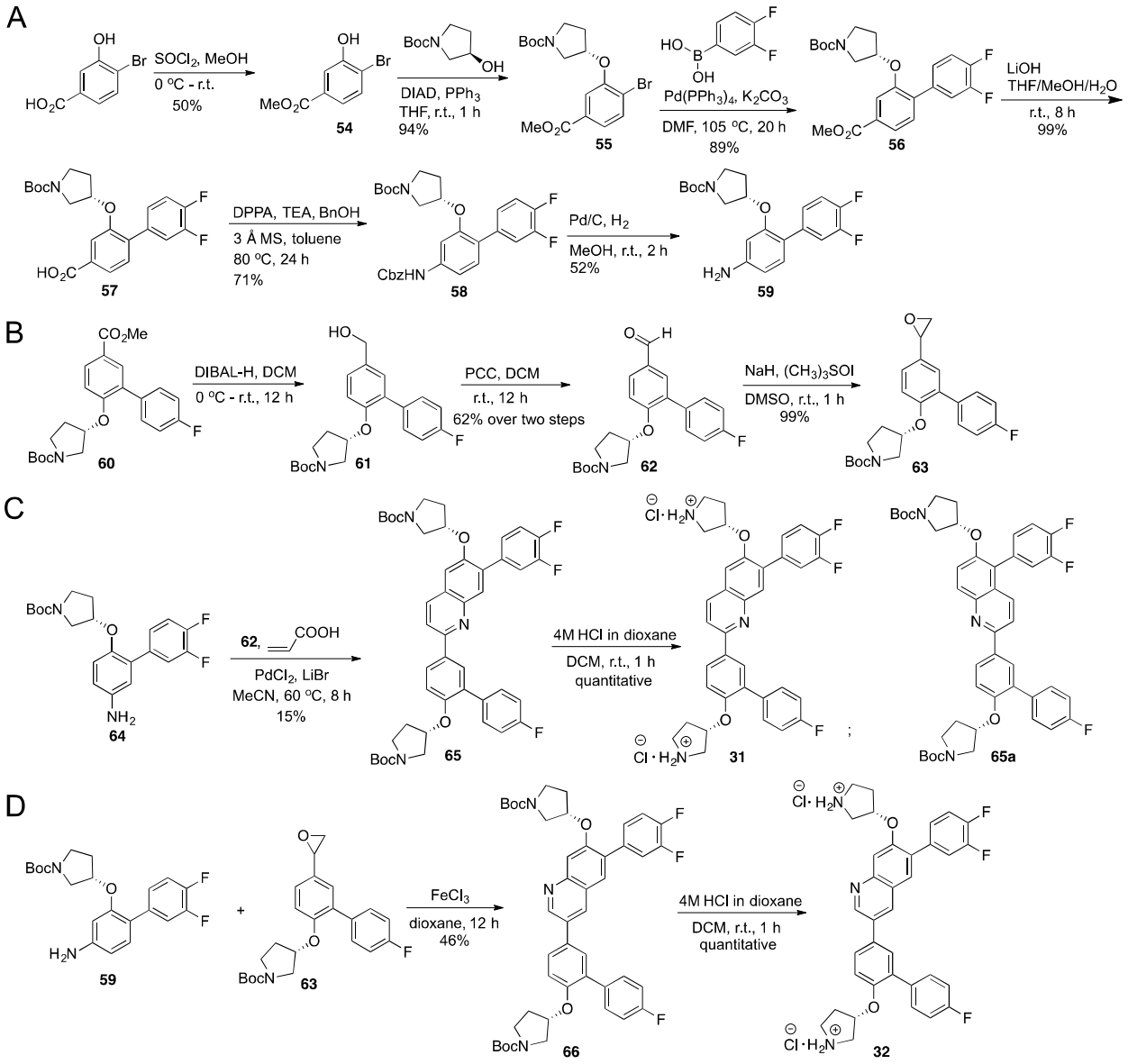

DISCUSSION

Wnt/*β*-catenin signaling is frequently observed hyperactive in cancers. The most effective target to develop anticancer inhibitors for the Wnt/*β*-catenin signaling pathway is the *β*-catenin-containing transcriptional complex, because this complex mediates the signaling at the downstream node in the pathway. However, despite numerous efforts, this target has proven to be challenging.[62] To date, only one series of drug-like inhibitors targets this transcriptional

complex, ICG-001 and its second-generation prodrug PRI-724.[63] PRI-724 is in clinical trial phase II.[64] ICG-001 and PRI-724 bind with transcription coactivator CBP to disrupt the *β*-catenin/CBP interaction.[65] In the structure of the *β*-catenin-containing transcriptional complex, the *β*-catenin/BCL9 PPI represents an unique target for inhibitor design because: (1) BCL9/B9L acts as an essential adaptor protein to recruit other cofactors and load *β*-catenin to the Wnt enhancesome, facilitating the access of *β*-catenin to Tcf/Lef.[33] The *β*-catenin/BCL9 PPI is required for transcription of Wnt responsive genes[32,39,40,66–69] and tumorigensis[41–43,70–72]; (2) this PPI has a moderately strong binding affinity (K_D = 0.47 μM); and (3) the *β*-catenin interface for binding with BCL9 is relatively small and has little overlap with those for the other *β*-catenin partners. Along with the efforts of the other groups to discover *β*-catenin/BCL9 inhibitors,[35,44–46] we reported the design and synthesis of **1** as a new small-molecule inhibitor for this PPI.[47]

In process of inhibitor optimization, we found that the gain of potency was limited by exploration of the hydrophobic interaction based on **1**. Also, the more hydrophobic compounds cause cytotoxicity by damaging the cell membrane, as evident in the LDH release assay. The substitution of the CH group of the aromatic rings of **1** with a N atom made the positive impact on the molecular and physiological properties of **12**–**14**, which displayed the lower cytotoxicity in the LDH release assay. However, none of them were more potent than **1**. Compound **1** is a lipophilic base. The previous bioinformatic analyses indicated that the lipophilic bases were prone to causing target promiscuity.[73–76] Hence, in process of improving inhibitor potency and selectivity for the Wnt/*β*-catenin signaling pathway, we also aimed to introduce the polar groups; compound **29** was obtained. This compound exhibits a K_i of 0.47 μM for disruption of the *β*-catenin/BCL9 PPI and >1900-fold selectivity for *β*-catenin/BCL9 over *β*-catenin/E-cadherin PPIs in biochemical AlphaScreen assays. This compound dose-dependently inhibited TOPFlash

luciferase reporter activity with an IC_{50} of 25 μM, did not exhibit cytotoxicity in the LDH release assay, and had no effect on FOPFlash luciferase reporter activity up to the concentration of 200 μM.

The K_i of **29** for disruption of the β-catenin/BCL9 PPI was 0.47 μM. The TOPFlash luciferase reporter (with three Tcf binding sites) activity of **29** was 25 μM. This difference could be caused by the zwitterion nature of this compound. The intracellular concentration of **29** was determined by the method described in the previous study.[48] The result was shown in the Supplementary Note. The cell-bound concentration of **29** at 37 °C was determined to be 6.6 nmol/million HCT116 cells for the 6 h incubation in 5 mL of DMEM media with 10% FBS, when the input concentration was 50 μM of **29**. The 4 °C incubation experiment indicated a significant amount (77%) of cell-bound **29** bound with the cell membrane through the nonspecific manner. The cell-bound concentration of **29** was 5.1 nmol/million HCT116 cells for 6 h incubation at 4 °C in 5 mL of DMEM media with 10% FBS. This result is different from that of **1**.[48] The cell-bound concentration of **1** at 37 °C was determined to be 6.7 nmol/million MDA-MB-231 cells for the 6 h incubation in 5 mL of DMEM media with 10% FBS, when the input concentration was 2 μM of **1**. At 4 °C, the cell-bound concentration of **1** was 1 nmol/million MDA-MB-231 cells for 6 h incubation at 4 °C in 5 mL of DMEM media with 10% FBS. Therefore, only 15% of **1** bound with the cell membrane by the nonspecific manner.

Four cancer cells were examined in cell-based studies. SW480 and HCT116 cells have hyperactive Wnt signaling. SW480 cells harbor the deletion of *APC*,[77] whereas HCT116 cells harbor the heterozygous three-base deletion of *CTNNB1*[78] that blocks β-catenin phosphorylation and ubiquitination. Although the expression levels of β-catenin in MDA-MB-231 cells are low,[79–81] MDA-MB-231 cells have high expression levels of upstream Wnt effectors, low-

density lipoprotein-related proteins 5 and 6 (LRP 5/6),[81,82] frizzled (Fzd),[83,84] and dishevelled.[79] MDA-MB-231 cells are susceptible to the activation by Wnt ligands to promote cancer cell growth *in vitro* and *in vivo*.[83,85] *β*-Catenin siRNA knocks down *β*-catenin expression in MDA-MB-231 cells and blocks cancer cell migration and invasion.[80,86] These three cancer cell lines were chosen based on their dependence on *β*-catenin for growth and survival. On the other hand, A549 cells do not contain active Wnt/*β*-catenin signaling.[87,88]

In this study, the tetrazolium MTS assay was used to examine the inhibitory effects of new compounds on cancer cell viability. The MTS assay, however, cannot distinguish the effects on cell death and cell growth inhibition. LDH release was used as the preferred biomarker to examine the effect on cell death because LDH is a soluble cytoplasmic enzyme that is present in all examined cells of this study. It is released to the extracellular space when the cytoplasmic membrane is damaged. Through the combinational use of the MTS (compounds were incubated with cancer cells for 72 h) and LDH release (compounds were incubated with cancer cells for 4 h) assays, the effects of these compounds on cytotoxicity and on inhibition of the viability of cancer cells can be differentiated.

Compounds **2**–**18** displayed high activities in MTS assays. However, they also exhibited cytotoxicity in the LDH release assay. They are not suitable for the further inhibitor optimization. In contrast, compounds **24**–**30** inhibited growth of cancer cells in the MTS assays but had no effect on LDH release activity, indicating that the future inhibitor optimization should take into consideration decreasing compound hydrophobicity, and compound **29** can be used as the new starting point. Compound **29** also exhibits selectivity on inhibiting the viability of Wnt-activated cancer cells over the cancer cells that have normal Wnt signaling. It is interesting that

the IC_{50} of **29** for the inhibition of TOPFlash luciferase reporter activity is lower than that for the MTS assay.

Similar to carnosic acid[35] and **1**[47], compounds **3** and **29** also selectively decrease the level of active form of *β*-catenin (i.e., nuclear *β*-catenin) without affecting the level of total *β*-catenin (i.e., E-cadherin-bound *β*-catenin). With the result that **29** disrupts the *β*-catenin/BCL9 interaction in co-IP experiments (Figures 8C,D), there are at least two possible mechanisms why **29** promotes the selective degradation of nuclear *β*-catenin. One is that **29** disrupts the interaction of *β*-catenin with BCL9, and free *β*-catenin is susceptible to the H1 (the first α-helix of *β*-catenin armadillo repeats)-dependent proteasomal degradation[35]. The second mechanism is that **29** binds with *β*-catenin after the disruption of the PPI, destabilizes *β*-catenin tertiary structure, and promotes *β*-catenin degradation. The further mechanistic studies are required to address this question.

Although **29** is more potent and selective than **1** in biochemical assays, it should be noted that **29** still has multiple carboaromatic rings, which are often considered to be the potential risk of the high serum albumin binding, and the inhibition of cytochrome P450 and human ether-a-go-go-related gene product (hERG), potentially lowering the developability of the compound.[89–92] In addition to improving inhibitor potency and maintaining inhibitor selectivity, the further optimization will be centered on the replacement of the aromatic rings with the aliphatic alternatives and the increase of the three-dimensional features of the designed compounds.

CONCLUSION

The Wnt/*β*-catenin signaling pathway is frequently implicated in tumorigenesis of many cancers. The pathway is not only involved in the proliferation of cancer cells, but more

importantly responsible for cancer progression, metastasis, and drug resistance. The activation of *β*-catenin signaling also blocks recruitment of cytotoxic T cells, promotes Treg cell survival and infiltration, and excludes anticancer immunity. On the other hand, it has been proven difficult to discover inhibitors for the downstream effectors of the Wnt/*β*-catenin signaling pathway. The *β*-catenin/BCL9 PPI in the transcriptional complex is an interesting target for chemical probe development and drug discovery. In this study, structure-based design and synthesis was conducted to optimize the inhibitors based on the 4'-fluoro-*N*-phenyl-[1,1'-biphenyl]-3-carboxamide scaffold. Compound **29** was found to disrupt the *β*-catenin/BCL9 PPI with a K_i of 0.47 μM and exhibited high selectivity (>1900-fold) for *β*-catenin/BCL9 over *β*-catenin/E-cadherin PPIs in the biochemical AlphaScreen assays. The site-directed mutagenesis studies indicated that *β*-catenin D145, E155, and K181 are important for the inhibitors to disrupt the *β*-catenin/BCL9 PPI. The cell-based studies indicated that **29** can selectively inhibit growth of cancer cells that have hyperactive Wnt/*β*-catenin signaling and did not show cytotoxicity in the LDH release assays. The co-IP experiments indicated that this compound disrupted the full-length *β*-catenin/BCL9 PPI while leaving the *β*-catenin/E-cadherin PPIs unaffected. The TOPFlash/FOPFlash luciferase reporter assays indicated that **29** can selectively suppress transactivation of Wnt/*β*-catenin signaling. This compound also downregulated expression of Wnt target genes in dose-dependent manners at both mRNA and protein levels, and only inhibited the downstream nodes of the Wnt/*β*-catenin signaling pathway. This study offered the directions for future inhibitor optimization.

EXPERIMENTAL SECTION

Chemical Synthesis.

General Methods, Reagents, and Materials. All reagents were purchased from the commercial sources and used without further purification unless stated otherwise. ^{1}H NMR and ^{13}C NMR spectra were recorded on the Bruker AVANCEIIIHD™ 500 (500 MHz), Varian VXR-500 (500 MHz), Varian Inova-400 (400 MHz), or Varian Unity-300 (300 MHz) spectrometers (125.7 MHz, 125.7 MHz, 100 MHz, and 75 MHz for ^{13}C NMR spectra, respectively) in d^6-DMSO, d^6-acetone, d^4-methanol, and $CDCl_3$. Chemical shifts were reported as values in parts per million (ppm), and the reference resonance peaks were set at 7.26 ppm ($CHCl_3$), 3.31 ppm (CD_2HOD), 2.50 ppm [$(CD_2H)_2SO$], 2.05 ppm [$(CD_2H)_2CO$] for the ^{1}H NMR spectra and 77.23 ppm ($CDCl_3$), 49.00 ppm (CD_3OD), 39.52 ppm (d^6-DMSO), and 29.84 ppm (d^6-acetone) for the ^{13}C NMR spectra. Low-resolution mass spectra were determined on the Agilent 6120 single quadrupole MS with 1220 infinity LC system (HPLC-MS) with an ESI source. High-resolution mass spectra were determined on the Agilent G6230BA TOF LCMS Mass Spectrometer with a TOF mass detector. Thin-layer chromatography was carried out on E. Merck pre-coated silica gel 60 F254 plates with visualization accomplished with phosphomolybdic acid and ninhydrin spray reagents, or with a UV–visible lamp. Column chromatography was performed with SilicaFlash$^{@}$ F60 (230–400 mesh). The purity of final compounds **2**–**32** was determined by HPLC analysis with two different conditions. The instrument was an Agilent 1260 Infinity II HPLC system with a quaternary pump, a vial sampler, and a diode array detector (DAD). A Kromasil 300–5–C18 column (4.6 × 250 mm) was used. The DAD detector was set to 220, 254, and 280 nm. The purity of all tested compounds was ≥ 95%.

***N*-(4'-Fluoro-6-(((*S*)-pyrrolidin-3-yl) oxy)-[1,1'-biphenyl]-3-yl)-3-(6-fluoronaphthalen-2-yl)-4-(((*S*)-pyrrolidin-3-yl) oxy) benzamide dihydrochloride (2).** To a solution of **36a** (0.40 g, 0.50 mmol) in CH_2Cl_2 (2 mL) under the anhydrous condition was added 4 M HCl in dioxane (10 mL). The mixture was then stirred at room temperature for 1–1.5 h. The solvent was removed under the reduced pressure to yield **2** as white solid (0.27 g, 88%). ^{1}H NMR (500 MHz, CD_3OD) δ 8.09–7.91 (m, 4H), 7.86 (d, *J* = 8.5 Hz, 1H), 7.76–7.52 (m, 6H), 7.38–6.96 (m, 5H), 5.26 (s, 1H), 5.02 (s, 1H), 3.86–3.37 (m, 6H), 3.19 (dq, *J* = 30.1, 10.7, 10.2 Hz, 2H), 2.53–2.03 (m, 4H). ^{13}C NMR (126 MHz, CD_3OD) δ 166.60, 163.34, 162.01, 161.39, 160.06, 156.52, 150.25, 134.67, 134.65, 134.25, 134.22, 133.62, 133.55, 133.46, 131.46, 131.37, 131.32, 131.26, 131.19, 130.95, 130.89, 130.82, 130.70, 128.91, 128.80, 128.28, 128.22, 126.87, 126.83, 124.29, 123.13, 121.91, 120.75, 116.26, 116.06, 115.80, 115.58, 114.93, 114.76, 113.57, 110.41, 110.24, 77.33, 76.71, 50.61, 44.44, 44.27, 31.05, 30.82. HRMS (ESI) Calcd for $C_{37}H_{33}F_2N_3O_3$ $(M+H)^+$ 606.2568, found 606.2554.

3-(Benzo[*b*]thiophen-6-yl)-*N*-(4'-fluoro-6-(((*S*)-pyrrolidin-3-yl) oxy)-[1,1'-biphenyl]-3-yl)-4-(((*S*)-pyrrolidin-3-yl) oxy) benzamide dihydrochloride (3). It was prepared through the same procedure for **2** to yield **3** as white solid (83% yield). ^{1}H NMR (300 MHz, CD_3OD) δ 8.07 (d, *J* = 1.5 Hz, 1H), 7.99 (d, *J* = 8.3 Hz, 2H), 7.88 (d, *J* = 8.3 Hz, 1H), 7.74–7.65 (m, 2H), 7.67–7.45 (m, 4H), 7.39 (d, *J* = 5.5 Hz, 1H), 7.23 (d, *J* = 8.4 Hz, 1H), 7.13 (td, *J* = 9.7, 9.3, 5.7 Hz, 3H), 5.25 (s, 1H), 5.02 (d, *J* = 3.5 Hz, 1H), 3.49 (dddt, *J* = 35.8, 31.2, 11.3, 5.3 Hz, 6H), 3.18 (ddt, *J* = 20.0, 11.6, 8.3 Hz, 2H), 2.46–2.07 (m, 4H). ^{13}C NMR (75 MHz, CD_3OD) δ 166.67, 156.51, 150.25, 140.03, 139.19, 134.24, 133.79, 133.46, 131.78, 131.48, 131.32, 131.22, 130.96, 128.70, 128.24, 127.15, 126.03, 124.28, 123.53, 123.05, 123.00, 121.88, 115.57, 114.97, 114.69, 113.76, 77.36,

76.82, 50.62, 44.40, 44.26, 31.04, 30.82. HRMS (ESI) Calcd for $C_{35}H_{32}FN_3O_3S$ $(M+H)^+$ 594.2227, found 594.2217.

3',4'-Difluoro-6-((*S*)-pyrrolidin-3-yloxy)-*N*-(6-((*S*)-pyrrolidin-3-yloxy)-3'-(2H-tetrazol-5-yl)-[1,1'-biphenyl]-3-yl)-[1,1'-biphenyl]-3-carboxamide dihydrochloride (27). It was prepared through the same procedure as **2** to afford **27** as white solid (76% yield). ^{1}H NMR (500 MHz, CD_3OD): δ ppm 8.30 (s, 1H), 8.03 (dd, J = 2.5 Hz, 9.0 Hz, 1H), 7.99–7.97 (m, 2H), 7.80–7.72 (m, 3H), 7.65 (t, J = 8.0 Hz, 1H), 7.57–7.47 (m, 1H), 7.41–7.30 (m, 2H), 7.26 (d, J = 9.0 Hz, 1H), 7.19 (d, J = 9.0 Hz, 1H), 5.31 (s, 1H), 5.14 (s, 1H), 3.66–3.62 (m, 1H), 3.56–3.52 (m, 3H), 3.52–3.37 (m, 3H), 3.29–3.23 (m, 1H), 2.39–2.17 (m, 4H). ^{13}C NMR (125 MHz, CD_3OD): δ ppm 166.17, 156.00, 150.08, 139.11, 133.20, 131.94, 130.67, 130.39, 129.28, 129.11, 129.05, 128.00, 125.94, 125.91, 125.89, 125.46, 124.20, 124.02, 122.16, 118.26, 118.12, 116.76, 116.62, 114.84, 113.24, 109.99, 76.90, 76.52, 50.48, 50.36, 44.23, 44.10, 30.75, 30.66. HRMS (ESI) Calcd for $C_{34}H_{31}F_2N_7O_3$ $(M+H)^+$ 624.2535, found 624.2528.

3',4'-Difluoro-6-((*S*)-pyrrolidin-3-yloxy)-*N*-(6-((*S*)-pyrrolidin-3-yloxy)-4'-(2H-tetrazol-5-yl)-[1,1'-biphenyl]-3-yl)-[1,1'-biphenyl]-3-carboxamide dihydrochloride (28). It was prepared through the same procedure as **2** to afford **28** as white solid (80% yield). ^{1}H NMR (500 MHz, CD_3OD): δ ppm 8.09 (dd, J = 2.0 Hz, 8.5 Hz, 2H), 8.03 (dd, J = 2.0 Hz, 8.5 Hz, 1H), 8.00–7.97 (m, 1H), 7.76 (dd, J = 3.0 Hz, 9.0 Hz, 1H), 7.74–7.66 (m, 3H), 7.57–7.46 (m, 1H), 7.39–7.29 (m, 2H), 7.25 (d, J = 8.5 Hz, 1H), 7.17 (d, J = 8.5 Hz, 1H), 5.31 (s, 1H), 5.08 (s, 1H), 3.65–3.62 (m, 1H), 3.56–3.43 (m, 4H), 3.41–3.33 (m, 1H), 3.29–3.22 (m, 1H), 3.20–3.11 (m, 1H), 2.40–2.25 (m, 2H), 2.25–2.11 (m, 2H). ^{13}C NMR (125 MHz, CD_3OD): δ ppm 156.00, 150.20, 139.59, 133.38, 131.73, 130.38, 129.37, 129.05, 128.15, 126.40, 126.18, 125.82, 123.94, 121.99, 118.27,

118.12, 116.78, 116.64, 115.59, 113.26, 77.37, 76.53, 50.54, 50.41, 44.22, 44.04, 30.70, 30.48. HRMS (ESI) Calcd for $C_{34}H_{31}F_2N_7O_3$ $(M+H)^+$ 624.2535, found 624.253.

3',4'-Difluoro-6-(((*S*)-pyrrolidin-3-yl) oxy)-*N*-(6-(((*R*)-pyrrolidin-3-yl) oxy)-3'-(2*H*-tetrazol-5-yl)-[1,1'-biphenyl]-3-yl)-[1,1'-biphenyl]-3-carboxamide dihydrochloride (29). It was prepared through the same procedure as **2** to afford **29** as white solid (85% yield). ^{1}H NMR (500 MHz, DMSO-d_6) δ 10.26 (s, 1H), 9.40 (d, *J* = 32.9 Hz, 4H), 8.29 (s, 1H), 8.06 (d, *J* = 7.4 Hz, 1H), 8.01 (d, *J* = 6.6 Hz, 2H), 7.84 (d, *J* = 11.8 Hz, 2H), 7.74 (d, *J* = 8.2 Hz, 2H), 7.66 (d, *J* = 7.6 Hz, 1H), 7.48 (q, *J* = 4.5, 3.3 Hz, 2H), 7.27 (d, *J* = 8.5 Hz, 1H), 7.18 (d, *J* = 8.6 Hz, 1H), 5.23 (s, 1H), 5.06 (s, 1H), 3.59–3.06 (m, 8H), 2.23–2.00 (m, 4H). ^{13}C NMR (126 MHz, CD_3OD) δ 166.10, 156.13, 150.57, 150.11, 148.66, 139.12, 134.51, 133.13, 133.06, 130.94, 130.56, 130.45, 130.25, 129.33, 128.27, 127.93, 127.13, 125.94, 124.51, 123.79, 123.26, 119.02, 117.90, 117.41, 116.41, 78.56, 54.58, 54.13, 47.35, 46.93, 33.64, 33.14. HRMS (ESI) Calcd for $C_{34}H_{31}F_2N_7O_3$ $(M+H)^+$ 624.2535, found 624.253.

(*R*)-3-((5-(3-(Benzo[*b*]thiophen-6-yl)-4-(((*S*)-pyrrolidin-1-ium-3-yl) oxy) benzamido)-3'-(2*H*-tetrazol-5-yl)-[1,1'-biphenyl]-2-yl) oxy) pyrrolidin-1-ium chloride (30). It was prepared through the same procedure as **2** to afford **30** as white solid (82% yield). ^{1}H NMR (500 MHz, DMSO-d_6) δ 10.29 (s, 1H), 9.53 (t, *J* = 59.7 Hz, 4H), 8.35 (t, *J* = 1.8 Hz, 1H), 8.29 (d, *J* = 1.4 Hz, 1H), 8.17–8.08 (m, 2H), 8.05 (dd, *J* = 8.7, 2.4 Hz, 1H), 7.95 (d, *J* = 8.3 Hz, 1H), 7.91–7.85 (m, 2H), 7.83–7.74 (m, 2H), 7.71–7.63 (m, 2H), 7.50 (d, *J* = 5.5 Hz, 1H), 7.32 (d, *J* = 8.8 Hz, 1H), 7.21 (d, *J* = 9.0 Hz, 1H), 5.27 (t, *J* = 5.0 Hz, 1H), 5.17–5.00 (m, 1H), 3.65–3.46 (m, 2H), 3.34 (m, 4H), 3.13 (d, *J* = 9.8 Hz, 2H), 2.27–2.01 (m, 4H). ^{13}C NMR (126 MHz, DMSO-d_6) δ 164.90, 156.35, 149.79, 139.70, 139.24, 138.99, 134.05, 133.82, 132.50, 131.08, 130.62, 129.94, 129.81, 129.34, 128.49, 128.19, 128.17, 126.67, 126.23, 124.17, 123.78, 123.71, 123.49, 121.80,

114.97, 113.76, 76.78, 76.53, 50.06, 50.01, 44.26, 44.12, 31.51, 31.40. HRMS (ESI) Calcd for $C_{36}H_{33}N_7O_3S$ $(M+H)^+$ 644.2444, found 644.2434.

7-(3,4-Difluorophenyl)-2-(4'-fluoro-6-((*S*)-pyrrolidin-3-yloxy)-[1,1'-biphenyl]-3-yl)-6-((*S*)-pyrrolidin-3-yloxy) quinoline dihydrochloride (31). The same procedure to prepare **2** was used to prepare **31** and yield yellow solid (quantitative yield). ^{1}H NMR (500 MHz, CD_3OD): δ ppm 8.76 (d, J = 10.5 Hz, 1H), 8.25 (d, J = 8.5 Hz, 1H), 8.22–8.15 (m, 3H), 7.76 (s, 1H), 7.68–7.61 (m, 3H), 7.51–7.46 (m, 1H), 7.45–7.38 (m, 2H), 7.21 (t, J = 9.0 Hz, 2H), 5.46 (s, 1H), 5.35 (s, 1H), 3.77–3.71 (m, 1H), 3.68–3.43 (m, 6H), 3.28–3.24 (m, 1H), 2.49–2.29 (m, 4H). ^{13}C NMR (126 MHz, CD_3OD) δ 163.46, 161.50, 156.87, 153.61, 152.91, 151.41, 149.53, 143.38, 138.19, 135.57, 133.16, 132.98, 131.91, 131.42, 131.32, 131.25, 129.79, 128.51, 126.36, 125.73, 123.61, 121.30, 118.64, 118.51, 117.23, 117.10, 114.85, 114.68, 114.48, 108.75, 102.74, 77.09, 76.76, 50.42, 50.21, 44.32, 44.25, 30.77, 30.65. HRMS (ESI) Calcd for $C_{35}H_{30}F_3N_3O_2$ $(M+H)^+$ 582.2368, found 582.2345.

6-(3,4-Difluorophenyl)-3-(4'-fluoro-6-((*S*)-pyrrolidin-3-yloxy)-[1,1'-biphenyl]-3-yl)-7-((*S*)-pyrrolidin-3-yloxy) quinoline dihydrochloride (32). The same procedure for **2** was used to prepare **32** to obtain yellow solid (quantitative yield). ^{1}H NMR (500 MHz, CD_3OD): δ ppm 9.41 (s, 1H), 9.12 (brs, 1H), 8.23 (s, 1H), 7.90 (dd, J = 2.5, 8.5 Hz, 1H), 7.86 (d, J = 2.0 Hz, 1H), 7.68 (s, 1H), 7.67–7.60 (m, 3H), 7.49–7.39 (m, 2H), 7.36 (d, J = 8.5 Hz, 1H), 7.20 (t, J = 9.0 Hz, 2H), 5.55 (s, 1H), 5.26 (s, 1H), 3.80 (dd, J = 5.0 Hz, 13.0 Hz, 1H), 3.69–3.58 (m, 2H), 3.57–3.50 (m, 2H), 3.48–3.42 (m, 1H), 3.38–3.33 (m, 1H), 3.27–3.21 (m, 1H), 2.57–2.40 (m, 2H), 2.31–2.26 (m, 2H). ^{13}C NMR (500 MHz, CD_3OD): 163.35, 161.39, 157.33, 154.25, 144.86, 134.06, 133.70, 133.68, 132.10, 131.20, 131.13, 130.99, 129.83, 127.57, 126.24, 126.21, 126.19, 118.59, 118.44,

117.06, 116.92, 115.16, 114.75, 114.58, 77.27, 76.78, 50.50, 50.21, 44.36, 44.17, 30.67, 30.56. HRMS (ESI) Calcd for $C_{35}H_{30}F_3N_3O_2$ $(M+H)^+$ 582.2368, found 582.2348.

***tert*-Butyl (*S*)-3-((5-(3-bromo-4-(((*S*)-1-(*tert*-butoxycarbonyl) pyrrolidin-3-yl) oxy) benzamido)-4'-fluoro-[1,1'-biphenyl]-2-yl) oxy) pyrrolidine-1-carboxylate (35).** To a solution of **33**[59] (1.0 g, 2.6 mmol) in CH_2Cl_2 (30 ml) was added **34**[47] (0.97 g, 2.6 mmol), EDC•HCl (0.75 g, 3.9 mmol), and DMAP (0.32 g, 2.6 mmol). The mixture was then stirred at room temperature for 24 h. The reaction mixture was diluted with CH_2Cl_2 (20 mL), washed with water (30 mL), brine (30 mL), and dried over $MgSO_4$. The solid was filtered, and the solvent was removed under the reduced pressure. The residue was then purified by column chromatography to yield **35** as white solid (1.3 g, 70%) ^{1}H NMR **(**500 MHz, acetone-d_6): δ ppm 8.91 (s, 1H), 7.62 (s, 1H), 7.41 (dd, J = 3.0, 9.0 Hz, 1H), 7.20 (s, 2H), 6.97–6.87 (m, 2H), 6.64 (d, J = 9.0 Hz, 1H), 6.57–6.52 (m, 3H), 4.63 (s, 1H), 4.38 (s, 1H), 3.12–2.73 (m, 8H), 2.70–2.54 (m, 1H), 1.72–1.52 (m, 2H), 0.82 (m, 18H). ^{13}C NMR (125 MHz, acetone-d_6): δ ppm 168.05, 163.53, 163.12, 161.18, 156.50, 154.08, 150.44, 134.78, 133.64, 132.81, 131.41, 131.18, 129.40, 128.75, 123.18, 120.90, 115.52, 114.91, 114.40, 112.48, 78.69, 78.50, 77.85, 77.05, 51.65, 51.54, 51.33, 51.17, 44.21, 43.95, 31.53, 31.37, 30.69, 30.36, 27.99.

***tert*-Butyl (*S*)-3-((5-(4-(((*S*)-1-(*tert*-butoxycarbonyl) pyrrolidin-3-yl) oxy)-3-(6-fluoronaphthalen-2-yl) benzamido)-4'-fluoro-[1, 1'-biphenyl]-2-yl) oxy) pyrrolidine-1-carboxylate (36a).** To a solution of **35** (0.50 g, 0.67 mmol) in dioxane/water (3:1 (v:v)) was added (6-fluoronaphthalen-2-yl) boronic acid (0.15 g, 0.80 mmol), Pd(dppf)Cl_2 (0.025 g, 0.034 mmol), and Na_2CO_3 (0.14 g, 1.3 mmol). The reaction mixture was heated to 90 °C under argon and stirred for 24 h. The reaction mixture was cooled to room temperature, diluted with ethyl acetate, washed with water and brine, and dried over Na_2SO_4. The solid was then filtered, and the

solution was concentrated under vacuum. The residue was purified by column chromatography to yield **36a** as white solid (0.40 g, 75% yield). ^{1}H NMR (500 MHz, acetone-d_6) δ 9.64 (s, 1H), 8.15 (dd, *J* = 13.7, 2.4 Hz, 1H), 8.07–7.95 (m, 3H), 7.97–7.82 (m, 3H), 7.72 (d, *J* = 8.5 Hz, 1H), 7.66–7.58 (m, 1H), 7.52 (tt, *J* = 5.6, 2.6 Hz, 2H), 7.36 (td, *J* = 8.9, 2.6 Hz, 1H), 7.29–7.20 (m, 1H), 7.12 (td, *J* = 11.1, 10.0, 7.6 Hz, 3H), 5.19 (d, *J* = 14.3 Hz, 1H), 4.96 (d, *J* = 9.5 Hz, 1H), 3.74–3.14 (m, 8H), 2.30–1.92 (m, 4H), 1.75–0.96 (m, 18H). ^{13}C NMR (126 MHz, acetone-d_6) δ 164.91, 163.09, 161.93, 161.14, 159.98, 156.89, 154.21, 154.16, 154.05, 150.32, 150.26, 135.16, 135.04, 134.80, 133.88, 133.54, 133.47, 131.42, 131.37, 131.25, 131.15, 131.07, 130.92, 130.75, 130.62, 129.11, 129.05, 128.44 (d, *J* = 1.2 Hz), 128.34, 127.00, 126.86, 123.15, 122.07, 120.95, 116.49, 116.29, 115.51, 115.31, 114.90, 114.78, 114.73, 113.73, 113.59, 110.79, 110.76, 110.63, 78.74, 78.56, 77.85, 77.31, 77.04, 76.55, 51.66, 51.58, 51.21, 44.34, 44.24, 44.10, 43.99, 31.45, 31.38, 30.61, 30.56, 29.99, 28.03, 28.01

***tert*-Butyl (*S*)-3-((5-(3-(benzo[*b*]thiophen-6-yl)-4-(((*S*)-1-(*tert*-butoxycarbonyl) pyrrolidin-3-yl) oxy) benzamido)-4'-fluoro-[1,1 '-biphenyl]-2-yl) oxy) pyrrolidine-1-carboxylate (36b).** It was prepared through the same procedure for **36a** to afford **36b** as white solid (83% yield). ^{1}H NMR (500 MHz, acetone-d_6) δ 9.63 (s, 1H), 8.40–7.97 (m, 3H), 7.99–7.78 (m, 3H), 7.67 (t, *J* = 5.2 Hz, 1H), 7.61–7.50 (m, 3H), 7.45 (d, *J* = 5.2 Hz, 1H), 7.24 (d, *J* = 8.5 Hz, 1H), 7.15–6.98 (m, 3H), 5.16 (d, *J* = 6.4 Hz, 1H), 5.03–4.84 (m, 1H), 3.79–3.12 (m, 8H), 2.40–1.94 (m, 4H), 1.58–1.31 (m, 18H). ^{13}C NMR (75 MHz, acetone-d_6) δ 165.00, 163.72, 160.48, 156.90, 154.26, 154.06, 150.26, 139.93, 139.03, 134.83, 134.28, 133.91, 131.45, 131.35, 131.18, 130.65, 128.95, 128.33, 127.41, 126.31, 123.96, 123.24, 121.00, 115.49, 115.29, 114.99, 114.71, 113.72, 78.76, 78.58, 77.82, 77.41, 77.01, 76.45, 51.60, 51.20, 44.36, 44.25, 44.05, 31.48, 31.37, 30.61, 28.04.

(*S*)-*tert*-Butyl-3-(4-(((benzyloxy)carbonyl) amino)-2-bromophenoxy) pyrrolidine-1-carboxylate (37). To a solution of **33** (0.39 g, 1.01 mmol) in dry toluene (20 mL) under the anhydrous conditions was added diphenylphosphoryl azide (DPPA) (0.28 g, 1.01 mmol), Et_3N (0.20 g, 2.02 mmol), benzyl alcohol (1.00 mL), and the activated molecular sieves (2 g). The mixture was stirred at room temperature for 10 min and then heated to 80 °C under nitrogen for 24 h. Upon completion, the molecule sieves were filtered and the solution was diluted with EtOAc (50 mL). The organic layer was washed with water (50 mL), brine (50 mL), and dried over $MgSO_4$. The solid was filtered, and the solvent removed under the reduced pressure. The residue was purified by column chromatography to yield **37** as white solid (0.30 g, 60% yield). ^{1}H NMR (500 MHz, $CDCl_3$): δ ppm 7.63 (s, 1H), 7.41–7.26 (m, 5H), 6.81 (d, J = 8.5 Hz, 2H), 5.18 (s, 2H), 4.82 (s, 1H), 3.64–3.50 (m, 4H), 2.24–2.15 (br.m, 1H), 2.08–1.99 (m, 1H), 1.46 (s, 9H). ^{13}C NMR (500 MHz, $CDCl_3$): δ ppm 154.89, 154.76, 153.73, 150.12, 136.21, 133.18, 128.81, 128.50, 124.58, 119.25, 116.68, 114.37, 79.19, 78.31, 67.28, 51.69, 44.04, 31.92, 28.74.

(*S*)-*tert*-Butyl-3-(4-amino-2-bromophenoxy) pyrrolidine-1-carboxylate (38). Compound **37** (1.69 g, 3.44 mmol) was dissolved in MeOH, and an aqueous solution of NaOH (3.6 g, 89.44 mmol) in 15 mL of water was added to the stirring mixture. The reaction was heated to 55 °C for 38 h. Upon completion, the reaction mixture was neutralized with HCl, and the organic solvent was removed. To the remaining aqueous layer was added saturated $NaHCO_3$. The organic layer was washed with EtOAc by three times. After the removal of the organic solvent, the dark brown solid was obtained (0.96 g, 78%). ^{1}H NMR (500 MHz, $CDCl_3$): δ ppm 6.89 (s, 1H), 6.74 (d, J = 14.0 Hz, 1H), 6.59–6.52 (m, 1H), 4.73 (s, 1H), 3.69–3.44 (m, 4H), 2.25–2.13 (m, 1H), 2.08–1.89 (m, 1H), 1.45 (s, 9H). ^{13}C NMR (500 MHz, $CDCl_3$): δ ppm 154.90, 146.45, 142.83, 128.63, 127.13, 120.05, 119.38, 115.21, 80.03, 79.16, 51.67, 44.08, 31.05, 28.75.

(*S*)-*tert*-Butyl-3-((5-((3-bromo-4-(((*S*)-1-(*tert*-butoxycarbonyl) pyrrolidin-3-yl) oxy) phenyl) carbamoyl)-3',4'-difluoro-[1,1'-biphenyl]-2-yl) oxy) pyrrolidine-1-carboxylate (40). Compound **39** (0.17 g, 0.41 mmol) was dissolved in anhydrous CH_2Cl_2 at 0 °C. EDC•HCl (0.16 g, 0.82 mmol) and HOAt (0.062 g, 0.41 mmol) were added. The reaction mixture was allowed to stir at 0 °C for 30 min before **38** (0.15 g, 0.41 mmol) and Et_3N (0.20 ml, 1.3 mmol) were added. The reaction was stirred overnight while warming up to room temperature. The reaction was quenched after 24 h with 1 M HCl. The aqueous layer was washed twice with EtOAc, and the solvent of the combined organic layers was removed under the reduced pressure. Flash column chromatography was used to purify **40** as white solid (0.18 g, 60% yield). ^{1}H NMR (500 MHz, $CDCl_3$): δ ppm 8.98–8.80 (m, 1H), 7.87–7.78 (m, 3H), 7.71–7.47 (m, 1H), 7.19 (t, J = 9.0 Hz, 1H), 7.12–7.04 (m, 2H), 7.00–6.72 (m, 2H), 4.91–4.80 (m, 2H), 3.69–3.40 (m, 7H), 3.37–3.23 (m, 1H), 2.23–1.99 (m, 4H), 1.42 (s, 18H). ^{13}C NMR (500 MHz, $CDCl_3$): δ ppm 165.19, 156.63, 156.38, 154.81, 150.77, 150.49, 148.81, 134.26, 133.49, 130.26, 129.63, 128.82, 127.73, 125.98, 125.61, 120.90, 118.55, 116.94, 116.07, 113.87, 113.22, 80.00, 79.69, 51.58, 51.01, 44.29, 43.80, 31.66, 30.94, 28.60, 28.51.

(*S*)-*tert*-Butyl-3-((5-(6-(((*S*)-1-(*tert*-butoxycarbonyl) pyrrolidin-3-yl) oxy)-3',4'-difluoro-[1,1'-biphenyl]-3-ylcarboxamido)-3'-cyano-[1,1'-biphenyl]-2-yl) oxy) pyrrolidine-1-carboxylate (41a). It was prepared through the same procedure as **36** to afford **41a** as white solid (30% yield). ^{1}H NMR (500 MHz, acetone-d_6): δ ppm 9.64 (s, 1H), 8.05–8.03 (m, 2H), 7.87–7.79 (m, 4H), 7.71 (d, J = 7.5 Hz, 1H), 7.59 (t, J = 7.5 Hz, 1H), 7.51–7.44 (m, 1H), 7.35–7.31 (m, 2H), 7.26 (d, J = 8.5 Hz, 1H), 7.15 (d, J = 9.0 Hz, 1H), 5.22–5.17 (m, 1H), 5.05–5.01 (m, 1H), 3.61–3.27 (m, 8H), 2.19–2.13 (m, 4H), 1.42 (s, 9H), 1.40 (s, 9H).

(*S*)-*tert*-Butyl-3-((5-(6-(((*S*)-1-(*tert*-butoxycarbonyl) pyrrolidin-3-yl) oxy)-3',4'-difluoro-[1,1'-biphenyl]-3-ylcarboxamido)-4'-cyano-[1,1'-biphenyl]-2-yl) oxy) pyrrolidine-1-carboxylate (41b). It was prepared through the same procedure as **36** to afford **41b** as white solid (50% yield). ^{1}H NMR (500 MHz, acetone-d_6): δ ppm 9.60 (s, 1H), 8.07–8.04 (m, 2H), 7.89–7.87 (m, 2H), 7.80 (d, J = 9.0 Hz, 2H), 7.72 (d, J = 8.5 Hz, 1H), 7.55–7.51 (m, 1H), 7.30 (d, J = 8.5 Hz, 1H), 7.19 (d, J = 8.0 Hz, 1H), 5.25–5.21 (m, 1H), 5.08–5.04 (m, 1H), 3.63–3.20 (m, 8H), 2.20–2.08 (m, 4H), 1.43 (s, 9H), 1.40 (s, 9H).

(*S*)-*tert*-Butyl-3-((5-(6-(((*S*)-1-(*tert*-butoxycarbonyl) pyrrolidin-3-yl) oxy)-3',4'-difluoro-[1,1'-biphenyl]-3-ylcarboxamido)-3'-(2H-tetrazol-5-yl)-[1,1'-biphenyl]-2-yl) oxy) pyrrolidine-1-carboxylate (42a). To a stirred solution of **41a** (0.05 g, 0.064 mmol) in anhydrous toluene (5 mL) was added *n*-Bu_3SnN_3 (0.064 g, 0.19 mmol). The resulting solution was refluxed for 24 h. Upon completion, the reaction mixture was diluted with EtOAc (50 mL), washed with brine (20 mL× 3), and dried over Na_2SO_4. The solid was filtered, and the solvent was removed under the reduced pressure. The residue was purified by column chromatography (DCM:MeOH = 15:1 – 10:1) to yield **42a** as pale yellow solid (0.03 g, 57% yield). ^{1}H NMR (300 MHz, acetone-d_6): δ ppm 9.75 (s, 1H), 8.31–8.06 (m, 3H), 7.98 (s, 1H), 7.94–7.90 (m, 1H), 7.86 (s, 1H), 7.71 (d, J = 7.8 Hz, 1H), 7.59 (t, J = 7.5 Hz, 1H), 7.53–7.337.28 (d, J = 7.8 Hz, 1H), 7.15 (d, J = 9.0 Hz, 1H), 5.24–5.19 (m, 1H), 5.05–4.98 (m, 1H), 3.66–3.24 (m, 8H), 2.30–2.10 (m, 4H), 1.43–1.35 (m, 18H). MS (ESI) m/z = 846.4 $[M + Na]^+$.

(*S*)-*tert*-Butyl-3-((5-(6-(((*S*)-1-(*tert*-butoxycarbonyl) pyrrolidin-3-yl) oxy)-3',4'-difluoro-[1,1'-biphenyl]-3-ylcarboxamido)-4'-(2H-tetrazol-5-yl)-[1,1'-biphenyl]-2-yl) oxy) pyrrolidine-1-carboxylate (42b). The procedure for **42a** was used to prepare **42b** as white solid (50% yield). ^{1}H NMR (500 MHz, acetone-d_6): δ ppm 9.67 (s, 1H), 8.14 (d, J = 8.0 Hz, 2H),

8.06–8.04 (m, 2H), 7.88–7.83 (m, 2H), 7.68 (d, *J* = 8.0 Hz, 2H), 7.52–7.44 (m, 1H), 7.35–7.30 (m, 2H), 7.26 (s, 1H), 7.14 (d, *J* = 8.0 Hz, 1H), 5.22–5.18 (m, 1H), 5.04–5.00 (m, 1H), 3.63–3.23 (m, 8H), 2.21–2.08 (m, 4H), 1.45–1.37 (m, 18H). MS (ESI) m/z = 846.4 $[M + Na]^+$.

***tert*-Butyl (*R*)-3-((3'-cyano-5-(methoxycarbonyl)-[1,1'-biphenyl]-2-yl) oxy) pyrrolidine-1-carboxylate (44).** It was prepared through the same procedure as **36** to afford **44** as white solid (91% yield). ^{1}H NMR (500 MHz, $CDCl_3$) δ 8.05 (dd, *J* = 8.6, 2.2 Hz, 1H), 7.99 (d, *J* = 2.2 Hz, 1H), 7.77 (t, *J* = 1.8 Hz, 1H), 7.72–7.67 (m, 1H), 7.62–7.58 (m, 1H), 7.49 (d, *J* = 7.8 Hz, 1H), 6.97 (d, *J* = 8.6 Hz, 1H), 5.10–4.91 (m, 1H), 3.90 (s, 3H), 3.64–3.49 (m, 3H), 3.34–3.26 (m, 1H), 2.17–2.06 (m, 2H), 1.44 (s, 9H). ^{13}C NMR (126 MHz, $CDCl_3$) δ 166.33, 157.42, 154.41, 138.58, 133.83, 132.91, 132.58, 131.53, 130.87, 129.15, 128.87, 123.52, 118.74, 112.75, 112.31, 79.78, 76.93 (d, *J* = 31.9 Hz), 52.13, 51.04, 44.07, 31.64, 28.45. MS (ESI) m/z = 445.2 $[M + Na]^+$.

***tert*-Butyl (*R*)-3-((5-amino-3'-cyano-[1,1'-biphenyl]-2-yl) oxy) pyrrolidine-1-carboxylate (47).** Compound **44** was hydrolyzed under the basic condition to yield **45** (93% yield), which was used in next step without further purification. MS (ESI) m/z = 431.2 $[M + Na]^+$.

The procedure to prepare **47** from **45** was the same as that of **38** from **33** to afford **47** as dark brown solid (65% yield in two steps). ^{1}H NMR (400 MHz, $CDCl_3$) δ 7.75 (s, 1H), 7.70 (d, *J* = 7.9 Hz, 1H), 7.57 (d, *J* = 7.6 Hz, 1H), 7.45 (t, *J* = 7.7 Hz, 1H), 6.82 (d, *J* = 8.5 Hz, 1H), 6.71 (t, *J* = 8.6 Hz, 2H), 4.62 (s, 1H), 4.05 (s, 2H), 3.63–3.30 (m, 3H), 3.19 (d, *J* = 8.6 Hz, 1H), 2.05–1.83 (m, 2H), 1.43 (s, 9H). ^{13}C NMR (101 MHz, $CDCl_3$) δ 154.46, 146.88, 140.48, 139.59, 133.83, 132.84, 131.04, 130.40, 128.66, 118.87, 117.78, 117.34, 116.44, 79.35, 78.46, 50.99 (d, *J* = 49.7 Hz), 43.84 (d, *J* = 44.0 Hz), 30.88, 28.43. MS (ESI) m/z = 402.2 $[M + Na]^+$.

***tert*-Butyl (*R*)-3-((5-(6-(((*S*)-1-(*tert*-butoxycarbonyl) pyrrolidin-3-yl) oxy)-3',4'-difluoro-[1,1'-biphenyl]-3-carboxamido)-3'-cyano-[1,1'-biphenyl]-2-yl) oxy) pyrrolidine-1-**

carboxylate (48). It was prepared through the same procedure as **40** to afford **48** as white solid (56% yield). ^{1}H NMR (400 MHz, $CDCl_3$) δ 7.82 (d, *J* = 21.3 Hz, 2H), 7.69 (d, *J* = 7.6 Hz, 3H), 7.56 (d, *J* = 8.2 Hz, 2H), 7.44 (d, *J* = 7.7 Hz, 1H), 7.25 (s, 1H), 7.14 (s, 2H), 6.91 (s, 2H), 4.94 (s, 1H), 4.81 (s, 1H), 3.90–3.04 (m, 8H), 2.11 (dd, *J* = 25.8, 17.1 Hz, 4H), 1.42 (d, *J* = 1.8 Hz, 18H). MS (ESI) m/z = 803.3 $[M + Na]^+$.

***tert*-Butyl (*R*)-3-((5-(6-(((*S*)-1-(*tert*-butoxycarbonyl) pyrrolidin-3-yl) oxy)-3',4'-difluoro-[1,1'-biphenyl]-3-carboxamido)-3'-(2*H*-tetrazol-5-yl)-[1,1'-biphenyl]-2-yl) oxy) pyrrolidine-1-carboxylate (49).** It was prepared through the same procedure as **42a** to afford **49** as white solid (35%). ^{1}H NMR (400 MHz, acetone-d_6) δ 8.47–8.26 (m, 1H), 8.17–8.05 (s, 2H), 7.85–7.05 (m, 10H), 5.25 (d, *J* = 33.5 Hz, 1H), 4.32 (dd, *J* = 5.6, 2.3 Hz, 1H), 3.77–3.25 (m, 8H), 2.45–2.03 (m, 4H), 1.46 (d, *J* = 11.4 Hz, 18H). MS (ESI) m/z = 846.4 $[M + Na]^+$, MS (ESI) m/z = 822.4 $[M - H]^-$.

***tert*-Butyl (*S*)-3-(2-(benzo[*b*]thiophen-6-yl)-4-(methoxycarbonyl) phenoxy) pyrrolidine-1-carboxylate (50)**. The procedure to prepare **50** was the same as that for **36** to afford **50** as white solid (89% yield). ^{1}H NMR (500 MHz, $CDCl_3$) δ 8.11 (d, *J* = 4.9 Hz, 1H), 8.01 (t, *J* = 7.9 Hz, 1H), 7.97 (dt, *J* = 1.5, 0.8 Hz, 1H), 7.83 (d, *J* = 8.3 Hz, 1H), 7.52–7.41 (m, 2H), 7.35 (dd, *J* = 5.4, 0.9 Hz, 1H), 6.97 (d, *J* = 8.7 Hz, 1H), 4.97 (tt, *J* = 4.4, 2.2 Hz, 1H), 3.90 (s, 3H), 3.82–3.25 (m, 4H), 2.22–1.95 (m, 2H), 1.43 (d, *J* = 11.9 Hz, 9H). ^{13}C NMR (126 MHz, $CDCl_3$) δ 166.70, 157.70, 154.52, 154.35, 139.80, 139.69, 138.63, 133.59, 133.48, 133.04, 131.58, 130.49, 126.89, 126.78, 125.97, 123.62, 123.39, 123.14, 123.03, 122.90, 113.05, 112.93, 79.59, 76.28, 74.98, 52.01, 51.48, 51.05, 44.19, 43.83, 31.65, 30.88, 28.48.

***tert*-Butyl (*R*)-3-((5-(3-(benzo[*b*]thiophen-6-yl)-4-(((*S*)-1-(*tert*-butoxycarbonyl) pyrrolidin-3-yl) oxy) benzamido)-3'-cyano-[1,1'-biphenyl]-2-yl) oxy) pyrrolidine-1-carboxylate (52)**. The

procedure for the hydrolysis of **50** to yield **51** was the same as that for the reparation of **38** (95% yield). Compound **51** was used directly in next step without further purification.

The procedure to prepare **52** was the same as that to prepare **40** and afforded **52** as white solid (60% yield). ^{1}H NMR (500 MHz, $CDCl_3$) δ 8.74 (dd, *J* = 102.4, 33.0 Hz, 1H), 8.00–7.79 (m, 3H), 7.79–7.58 (m, 5H), 7.50 (d, *J* = 7.7 Hz, 1H), 7.46–7.36 (m, 3H), 7.31 (d, *J* = 5.4 Hz, 1H), 7.14–6.67 (m, 2H), 4.85 (s, 1H), 4.77 (s, 1H), 3.61–2.98 (m, 8H), 2.11–1.83 (m, 4H), 1.41 (s, 18H). ^{13}C NMR (126 MHz, $CDCl_3$) δ 165.51, 156.87, 156.50, 154.74, 154.59, 154.37, 139.68, 139.13, 138.60, 133.94, 133.55, 132.84, 132.71, 131.59, 130.54, 130.45, 129.71, 128.67, 128.35, 128.08, 127.90, 127.68, 126.86, 125.93, 123.61, 123.07, 122.93, 121.82, 118.87, 114.85, 113.47, 113.29, 112.11, 111.96, 79.78, 79.60, 77.68, 76.18, 53.85, 53.46, 51.42, 50.94, 50.79, 44.27, 44.19, 43.79, 43.71, 31.59, 30.79, 28.46. MS (ESI) m/z = 823.3 $[M + Na]^+$.

***tert*-Butyl (*R*)-3-((5-(3-(benzo[*b*]thiophen-6-yl)-4-(((*S*)-1-(*tert*-butoxycarbonyl) pyrrolidin-3-yl) oxy) benzamido)-3'-(2*H*-tetrazol-5-yl)-[1,1'-biphenyl]-2-yl) oxy) pyrrolidine-1-carboxylate (53)**. It was prepared by the same procedure as that for **42** to afford **53** as white solid (37% yield). ^{1}H NMR (500 MHz, $CDCl_3$) δ 9.00 (t, *J* = 47.7 Hz, 1H), 8.23–7.53 (m, 6H), 7.46–7.17 (m, 6H), 6.73 (dt, *J* = 82.1, 29.1 Hz, 2H), 4.95–4.43 (m, 2H), 3.72–3.04 (m, 8H), 2.03–1.71 (m, 4H), 1.52–1.22 (m, 18H). ^{13}C NMR (126 MHz, $CDCl_3$) δ 156.87, 155.49, 155.03, 154.49, 150.59, 150.26, 139.60, 138.79, 138.58, 133.46, 132.30, 131.62, 130.88, 128.89, 128.42, 128.13, 127.56, 126.85, 126.36, 125.90, 124.13, 123.59, 123.08, 122.85, 122.22, 114.45, 113.32, 80.17, 79.80, 76.09, 53.82, 53.43, 51.54, 51.32, 51.08, 50.83, 44.36, 44.00, 43.86, 31.74, 31.56, 30.74, 29.70, 28.49, 28.40. MS (ESI) m/z = 866.3 $[M + Na]^+$.

Methyl 4-bromo-3-hydroxybenzoate (54). To a solution of 4-bromo-3-hydroxybenzoic acid (5.00 g, 13.80 mmol) in MeOH (30 mL) was added $SOCl_2$ (2.50 g, 20.70 mmol) dropwise over

10 min at 0–5 °C. The mixture was stirred for 3 h at room temperature. The solvent was then removed under the reduced pressure, and the residue was taken into EtOAc (150 mL). The solution was washed with aqueous Na_2CO_3 (50 mL and brine (50 mL× 3), and dried over Na_2SO_4. The inorganic solid was removed by filtrations, and the organic solvent removed under the reduced pressure to yield **54** as white solid (1.61 g, 50%). ^{1}H NMR (300 MHz, DMSO-d_6): δ ppm 10.74 (s, 1H), 7.62 (d, J = 8.1 Hz, 1H), 7.51 (d, J = 2.1 Hz, 1H), 7.28 (dd, J = 2.1, 8.1 Hz, 1H), 3.81 (s, 3H). ^{13}C NMR (75 MHz, DMSO-d_6): δ ppm 166.33, 154.99, 134.02, 130.70, 121.61, 116.98, 115.77, 52.99.

(*S*)-*tert*-Butyl 3-(2-bromo-5-(methoxycarbonyl) phenoxy) pyrrolidine-1-carboxylate (55). The synthesis of **55** follows the same procedure as that previously described[47] to afford **55** as white solid (94%). ^{1}H NMR (300 MHz, $CDCl_3$): δ ppm 7.59 (d, J = 8.7 Hz, 1H), 7.50 (d, J = 9.0 Hz, 2H), 4.99 (s, 1H), 3.89 (s, 3H), 3.63–3.58 (br.s, 4H), 2.24–2.10 (br.m, 2H), 1.44 (s, 9H). ^{13}C NMR (75 MHz, $CDCl_3$): δ ppm 166.43, 154.73, 153.94, 133.92, 130.64, 123.68, 119.53, 115.40, 79.78, 78.57, 52.63, 51.59, 44.34, 31.93, 31.15, 28.72.

(*S*)-*tert*-Butyl 3-((3',4'-difluoro-4-(methoxycarbonyl)-[1,1'-biphenyl]-2-yl) oxy) pyrrolidine-1-carboxylate (56). To a solution of **55** (1 g, 2.50 mmol) in dry DMF (25 mL) under the anhydrous condition was added (3,4-difluorophenyl) boronic acid (0.47 g, 3.00 mmol), $Pd(PPh_3)_4$ (0.14 g, 0.13 mmol), and K_2CO_3 (0.52 g, 3.75 mmol). The mixture was heated to 105 °C under argon and stirred for 20 h. Then, the reaction mixture was cooled to room temperature, diluted with ethyl acetate, washed with water and brine, dried over Na_2SO_4, and concentrated under vacuum. The residue was purified by column chromatography to yield **56** as yellow solid (0.96 g, 89% yield). ^{1}H NMR (300 MHz, $CDCl_3$): δ ppm 7.72 (dd, J = 1.8 Hz, 7.8

Hz, 1H), 7.59 (s, 1H), 7.36 (d, *J* = 8.1 Hz), 7.34–7.28 (m, 1H), 7.22–7.12 (m, 2H), 5.00–4.97 (m, 1H), 3.94 (s, 3H), 3.62–3.43 (br.m, 3H), 3.39–3.23 (m, 1H), 2.14–2.04 (m, 2H), 1.44 (s, 9H).

(*S*)-2-((1-(*tert*-Butoxycarbonyl) pyrrolidin-3-yl) oxy)-3',4'-difluoro-[1,1'-biphenyl]-4-carboxylic acid (57). To the solution of **56** (0.33 g, 0.75 mmol) in a solvent mixture (14 mL, THF:MeOH:H_2O = 4:2:1) was added LiOH (0.14 g, 6.00 mmol). The mixture was stirred for 8 h at room temperature. Then, the pH value was adjusted to 4–5 with HCl (1 M), diluted with water (50 mL), and extracted with EtOAc (50 mL× 3). The combined organic phase was dried over Na_2SO_4 and concentrated under vacuum to afford **57** as white solid (0.31 g, 99% yield). It was used directly in next step without further purification. ^{1}H NMR (300 MHz, $CDCl_3$): δ ppm 7.78 (d, *J* = 7.8 Hz, 1H), 7.64 (s, 1H), 7.39 (d, *J* = 8.1 Hz, 1H), 7.35–7.30 (m, 1H), 7.22–7.17 (m, 2H), 5.01 (s, 1H), 3.76–3.43 (br.m, 3H), 3.41–3.23 (m, 1H), 2.21–2.01 (m, 2H), 1.46 (s, 9H). ^{13}C NMR (75 MHz, $CDCl_3$): δ ppm 154.92, 153.87, 151.78, 135.31, 134.27, 131.22, 130.23, 125.77, 123.78, 118.83, 118.59, 117.26, 117.03, 115.14, 80.16, 51.40, 44.27, 28.67.

(*S*)-*tert*-Butyl 3-((4-amino-3',4'-difluoro-[1,1'-biphenyl]-2-yl) oxy) pyrrolidine-1-carboxylate (59). The procedure to prepare **58** was the same as that used to prepare **37**. To a solution of **58** (0.75 g, 1.42 mmol) in MeOH (20 ml) was added 10% Pd on activated carbon (0.07 g, 10% by weight). The air was evacuated and exchanged with the H_2 gas three times. The reaction mixture was allowed to stir under H_2 for 2 h and then filtered through celite. The solvent was removed under the reduced pressure to yield **59** (0.29 g, 52% yield). ^{1}H NMR (500 MHz, $CDCl_3$): δ ppm 7.08 (d, *J* = 8.0 Hz, 1H), 6.37 (d, *J* = 8.0 Hz, 1H), 6.25 (s, 1H), 4.79–4.76 (m, 1H), 3.78 (brs, 2H), 3.64–3.25 (m, 4H), 2.22–1.97 (m, 2H), 1.45 (s, 9H).

(*S*)-*tert*-Butyl 3-((4'-fluoro-5-formyl-[1,1'-biphenyl]-2-yl) oxy) pyrrolidine-1-carboxylate (62). To a solution of the previously reported **60**[47] (1.00 g, 2.41 mmol) in CH_2Cl_2 (30 mL) was

added DIBAL-H (3.61 mL, 1.0 M in THF) dropwise at –78 °C. The reaction mixture was allowed to rise to room temperature and stirred overnight. Then, the reaction mixture was quenched with NH_4Cl (15 mL), extracted with CH_2Cl_2 (50 mL× 3), and dried over Na_2SO_4. After the removal of the inorganic solid and the solvent, the residue was purified by column chromatography (hexanes:acetone = 5:1 – 3:1) to yield **61** as yellow oil (62% yield over two steps) (MS (ESI) m/z = 410.2 $[M + Na]^+$).

To the solution of **61** (0.60 g, 1.55 mmol) in CH_2Cl_2 (20 mL) was added PCC (1.00 g, 4.65 mmol). The resulting mixture was stirred at room temperature overnight, diluted with DCM (80 mL), washed with brine (20 mL× 3), and dried over Na_2SO_4. After the removal of the inorganic solid and the solvent, the residue was purified by column chromatography (hexane:acetone = 6:1 – 5:1) to yield **62** (0.58 g, 99% yield) as pale yellow oil. ^{1}H NMR (300 MHz, $CDCl_3$): δ ppm 9.96 (s, 1H), 7.89–7.85 (m, 2H), 7.45–7.39 (m, 2H), 7.12–7.02 (m, 3H), 5.04–4.99 (m, 1H), 3.70–3.23 (m, 4H), 2.15–2.09 (m, 2H), 1.45 (s, 9H). ^{13}C NMR (75 MHz, $CDCl_3$): δ ppm 190.97, 164.14, 160.87, 159.03, 154.65, 133.08, 132.77, 131.64, 131.37, 131.26, 131.15, 130.50, 115.42, 115.13, 113.35, 79.92, 51.52, 44.17, 28.68. MS (ESI) m/z = 408.2 $[M + Na]^+$.

(3*S*)-*tert*-Butyl-3-((4'-fluoro-5-(oxiran-2-yl)-[1,1'-biphenyl]-2-yl) oxy) pyrrolidine-1-carboxylate (63). To a solution of NaH (60% dispensed in mineral oil) (0.094 g, 2.34 mmol) in DMSO (15 mL) was added $(CH_3)_3SOI$. The resulting mixture was stirred at room temperature for 5 min. Then, the solution of **62** (0.30 g, 0.78 mmol) in DMSO (5 mL) was added slowly. The reaction mixture was stirred for another 1 h, and poured into ice water (50 mL), extracted with EtOAc (30 mL× 3), and dried over Na_2SO_4. The removal of the inorganic solid and the solvent yields **63** as colorless oil (0.32 g, >99% yield). ^{1}H NMR (500 MHz, $CDCl_3$): δ ppm 7.43–7.40 (m, 2H), 7.22–7.18 (m, 2H), 7.07–7.04 (m, 2H), 6.92 (d, J = 8.0 Hz, 1H), 4.80–4.84 (m, 1H),

3.87–3.84 (m, 1H), 3.60–3.19 (m, 4H), 3.16–3.13 (m, 1H), 2.85–2.80 (m, 1H), 2.07–1.99 (m, 2H), 1.44 (s, 9H).

(*S*)-*tert*-Butyl-3-((2-(6-(((*S*)-1-(*tert*-butoxycarbonyl) pyrrolidin-3-yl) oxy)-4'-fluoro-[1,1'-biphenyl]-3-yl)-7-(3,4-difluorophenyl) quinolin-6-yl) oxy) pyrrolidine-1-carboxylate (65). To a 25 mL of round bottom flask was charged a solution of **64** (0.050 g, 0.13 mmol) and **62** (0.049 g, 0.13 mmol) in MeCN (5 mL). Then, LiBr (0.011 g, 0.13 mmol), $PdCl_2$ (0.0020 g, 0.013 mmol), acrylic acid (0.019 g, 0.13 mmol) were added under the magnetic stirring. The resulting mixture was heated to 60 °C for 8 h, diluted with EtOAc (60 mL), washed with brine (20 mL× 3), and dried over Na_2SO_4. After the removal of the inorganic solid and the solvent, the residue was purified by column chromatography (hexanes:EtOAc = 2:1 – 1:1) to yield **65** as yellow solid (0.015 g, 15% yield). ^{1}H NMR (500 MHz, $CDCl_3$): δ ppm 8.12–8.08 (m, 4H), 7.85 (d, J = 8.5 Hz, 1H), 7.52 (dd, J = 5.5, 8.0 Hz, 2H), 7.47–7.40 (m, 1H), 7.32–7.30 (m, 1H), 7.24–7.19 (m, 1H), 7.12–7.06 (m, 4H), 5.06–5.03 (m, 1H), 4.96–4.93 (m, 1H), 3.78–3.23 (m, 8H), 2.23–2.04 (m, 4H), 1.46 (s, 9H), 1.44 (s, 9H). MS (ESI) m/z = 782.4 $[M + H]^+$, MS (ESI) m/z = 804.4 $[M + Na]^+$.

(*S*)-*tert*-Butyl-3-((3-(6-(((*S*)-1-(*tert*-butoxycarbonyl) pyrrolidin-3-yl) oxy)-4'-fluoro-[1,1'-biphenyl]-3-yl)-6-(3,4-difluorophenyl) quinolin-7-yl) oxy) pyrrolidine-1-carboxylate (66). To a 25 mL of round bottom flask equipped with a magnetic stirrer bar was charged with **59** (0.020 g, 0.050 mmol), **63** (0.039 g, 0.10 mmol), $FeCl_3$ (0.0024 g, 0.015 mmol), and dioxane (10 mL). The resulting mixture was heated to reflux overnight. After 12 h, the reactions mixture was diluted with EtOAc (60 mL), washed with brine (20 mL × 3) and dried over Na_2SO_4. After the removal of the inorganic solid and the solvent, the residue was purified by column chromatography (DCM:MeOH = 80:1–70:1) to yield **66** as yellow solid (0.018 g, 46%). ^{1}H NMR

(500 MHz, acetone-d_6): δ ppm 9.23 (s, 1H), 8.54 (s, 1H), 7.99 (s, 1H), 7.83–7.81 (m, 2H), 7.66–7.64 (m, 2H), 7.59–7.57 (m, 2H), 7.46–7.33 (m, 3H), 7.19 (t, J = 8.5 Hz, 2H), 5.37–5.34 (m, 1H), 5.19–5.14 (m, 1H), 3.73–3.78 (m, 8H), 2.38–2.10 (m, 4H), 1.44–1.40 (m, 18H). MS (ESI) m/z = 782.4 $[M + H]^+$.

Ligand docking using AutoDock 4.2. The same Autodock procedure described in the previous study[59] was used to dock **3** and **29**.

Protein expression and purification. Full-length β-catenin and (residues 1–781) were cloned into a pET-28b vector carrying a *C*-terminal 6 × histidine (Novagen), and transformed into *E. coli* BL21 DE3 (Novagen). Cells were cultured in LB medium with 30 μg/mL kanamycin until the OD_{600} was approximately 0.8, and then protein expression was induced with 400 μM of IPTG at 20 °C overnight. Cells were lysed by sonication. The proteins were purified by three steps of chromatography, including Ni-NTA affinity chromatography (30210, Qiagen), HiTrap Q HP anion exchange chromatography (17-1154-01, GE Healthcare Life Science), and size-exclusion chromatography with a HiLoad 26/600 Superdex 200 pg column (28-9893-36, GE Healthcare Life Science) using an AKTA Pure FPLC system (GE Healthcare Life Science). Protein was eluted in a buffer containing 20 mM of Tris (pH 8.5), 100 mM NaCl, and 2 mM DTT. The purity of β-catenin was greater than 95% as determined by SDS-PAGE gel analysis. Thermal-shift assay was performed on an CFX96 Real Time System (Bio-Rad) to monitor protein stability and detect protein aggregation. Protein unfolding was evaluated through measuring the fluorescence changes of fluorescent dye Sypro Orange when interacting with wild-type or mutant β-catenin proteins. A temperature increment of 1°/min was applied. All proteins were stable and no aggregation was observed under storage or assay conditions. Proteins were aliquoted and stored at –80 °C.

BCL9 peptide synthesis and purification. Human BCL9 (residues 350–375), *N*-terminally biotinylated human BCL9 (residues 350–375), human E-cadherin (residues 824–877), and *N*-terminally biotinylated human E-cadherin (residues 824–877) were synthesized by InnoPep Inc. (San Diego, CA, www.innopep.com). All synthesized peptides were purified by HPLC with purity >95%. The structures were validated by LC/MS. The sequences are as follows (Ahx, 6-aminohexanoic acid).

Peptide	Sequence
BCL9 26-mer	H-^{350}GLSQEQLEHRERSLQTLRDIQRMLFP^{375}-NH_2
Biotinylated BCL9 26-mer	Biotin-Ahx-^{350}GLSQEQLEHRERSLQTLRDIQRMLFP^{375}-NH_2
E-cadherin 54-mer	H-^{824}APPYDSLLVFDYEGSGSEAASLSSLNSSESDKDQDYDYLNEWGNRFKKLADMYG^{877}-NH_2
Biotinylated E-cadherin 54-mer	Biotin-^{824}APPYDSLLVFDYEGSGSEAASLSSLNSSESDKDQDYDYLNEWGNRFKKLADMYG^{877}-NH_2

AlphaScreen competitive inhibition assays. For the competitive inhibition assays of the β-catenin/BCL9 PPI, the negative control (equivalent to 0% inhibition) refers to 5.0 nM of biotinylated BCL9, 40 nM of His_6-tagged β-catenin, and 10 μg/mL of donor and acceptor beads in a final volume of 25 μL assay buffer, but no tested inhibitor present. The positive control (equivalent to 100% inhibition) refers to 5.0 nM of biotinylated BCL9 and 10 μg/mL of donor and acceptor beads in a final volume of 25 μL assay buffer. For the competitive inhibition assays of β-catenin/E-cadherin interactions, the negative control (equivalent to 0% inhibition) refers to 10 nM of biotinylated E-cadherin, 40 nM of His_6-tagged β-catenin, and 10 μg/mL of donor and acceptor

beads in a final volume of 25 μL assay buffer. The positive control (equivalent to 100% inhibition) of β-catenin/E-cadherin interactions refers to 10 nM of biotinylated E-cadherin and 10 μg/mL of donor and acceptor beads in a final volume of 25 μL assay buffer.

For the β-catenin/BCL9 assay, 5 nM of biotinylated BCL9 and 40 nM of His_6-tagged β-catenin were incubated in assay buffer at 4 °C for 30 min. For the β-catenin/E-cadherin assay, 10 nM of biotinylated human E-cadherin, and 40 nM of His_6-tagged human β-catenin were added and incubated in assay buffer at 4 °C for 30 min. Different concentrations of the tested inhibitor were added and incubated in 20 μL assay buffer at 4 °C for another 1 h. All of the above assay plates were covered and gently mixed on an orbital shaker. The donor and acceptor beads were then added to the plates to a final concentration of 10 μg/mL in 25 μL assay buffer. The mixture was incubated for 1 h at 4 °C before detection. The IC_{50} value was determined by nonlinear least-square analysis of GraphPad Prism 5.0. The K_i values were derived from the IC_{50} values using a method reported by Nikolovska-Coleska et al.[93] The assays were conducted under the conditions required by Nikolovska-Coleska *et al.*'s equation for determining the K_i values. All of the experiments were performed in triplicate. The results were expressed as mean ± standard deviation. The inhibitor selectivity for β-catenin/BCL9 over β-catenin/E-cahderin interactions was defined as the ratio of the respective K_i value of β-catenin/E-cadherin interactions over that of β-catenin/BCL9 interactions.

MTs cell viability assay. Colorectal cancer cell lines, SW480 and HCT116, triple-negative breast cancer cell line MDA-MB-231, and lung cancer cell line A549 were seeded in 96-well plates at 5 × 10^3 cells/well, maintained overnight at 37 °C, and incubated in the presence of inhibitors at various concentrations. Cell viability was monitored after 72 h using a freshly prepared mixture of 1 part phenazine methosulfate (PMS, Sigma) solution (0.92 mg/mL) and 19 parts MTs agent (3-

(4,5-dimethylthiazol-2-yl)-5-(3-carboxymethoxyphenyl)-2-(4-sulfophenyl)-2H-tetrazolium, inner salt, Promega) solution (2 mg/mL). Cells were incubated in 10 μL of this solution at 37 °C for 3 h, and A_{490} was measured. The effect of each compound is expressed as the concentration required to reduce A_{490} by 50% (IC_{50}) relative to vehicle-treated cells. Experiments were performed in triplicate.

LDH assay. The cytotoxic effects of the inhibitors on the cell membrane integrity were determined by measuring the activity of LDH using CytoTox 96® Non-Radioactive Cytotoxicity Assay (Promega). SW480 cells were seeded in 96-well plates at 2×10^4 cells/well, maintained overnight at 37 °C, and incubated in the presence of inhibitors at various concentrations. After 4 h incubation, the cell culture supernatant was incubated with diagnostic reagents in the LDH kit according to the manufacturer's instructions. The activity of LDH was calculated as the following equation after detection at 490 nm using Synergy 2 plate reader (Biotek). Percent cytotoxicity = 100 × (experimental release – background group)/(maximum release – background group). Experiments were performed in triplicate.

Cell transfection and luciferase assay. FuGENE6 (E269A, Promega) 96 well plate format was used for the transfection of HEK293 and SW480 cells according to the manufacturer's instruction. HEK293 cells were co-transfected with 45 ng of TOPFlash or FOPFlash reporter gene, 135 ng pcDNA3.1–β-catenin, and 20 ng of pCMV-RL normalization reporter gene. SW480 cells were co-transfected with 60 ng of the TOPFlash or FOPFlash reporter gene and 40 ng of pCMV-RL normalization reporter. Cells were cultured in DMEM and 10% FBS at 37 °C for 24 h, and different concentrations of inhibitors or DMSO was added. After 24 h, the luciferase reporter activity was measured using the Dual-Glo system (E2940, Promega). Normalized luciferase

activity in response to the treatment with inhibitors was compared with that obtained from the cells treated with DMSO. Experiments were performed in triplicate.

qPCR analysis. SW480 cells at 1 × 10^6/mL were treated with inhibitors at different concentrations for 24 h. Total RNAs were extracted with TRIzol (15596026, Life Technologies), and the cDNA was synthesized with the superscript III first-strand kit (18080-051, Invitrogen). qPCR experiments were performed using the iQ^{TM} SYBR green supermix kit (170-8880, BIO-RAD) on an CFX96 Real Time System (BIO-RAD). The threshold cycle (C_T) values were normalized to that of internal reference *GAPDH*. Experiments were performed in triplicate. The primer pairs are shown below

human *GAPDH*	forward	5′-GAAGGTGAAGGTCGGAGTC-3′
	reverse	5′-GAAGATGGTGATGGGATTTC-3′
human *HPRT*	forward	5′-GCTATAAATTCTTTGCTGACCTGCTG-3′
	reverse	5’-AATTACTTTTATGTCCCCTGTTGACTGG-3′
human *AXIN2*	forward	5′-AGTGTGAGGTCCACGGAAAC-3′
	reverse	5′-CTTCACACTGCGATGCATTT-3′
human *LEF1*	forward	5′-GACGAGATGATCCCCTTCAA-3′
	reverse	5′-AGGGCTCCT GAGAGGTTTGT-3′
human *cyclin D1*	forward	5′-ACAAACAGATCATCCGCAAACAC-3′
	reverse	5′-TGTTGGGGCTCCTCAGGTTC-3′

Western blotting. SW480 cells at 1 × 10^6 cells/mL were treated with different concentrations of inhibitors for 24 h. Cells were lysed in buffer containing 50 mM Tris (pH 7.4), 150 mM NaCl, 1% Nonidet P-40, 0.5% sodium deoxycholate, 0.1% SDS, and protease inhibitors. After centrifugation at 12,000 rpm for 20 min at 4 °C, the supernatant was loaded onto an 8% SDS

polyacrylamide gel for electrophoretic analysis. Separated proteins were transferred onto nitrocellulose membranes for immunoblot analysis. The antibodies against total *β*-catenin (610153, BD Biosciences, most of which is phosphorylated *β*-catenin and represents the E-cadherin bound pool), the active form of *β*-catenin (ABC, 05-665, EMD Millipore, dephosphorylated at positions S37 and T41 of *β*-catenin), cyclin D1 (sc-853, Santa Cruz Biotechnology, Inc.), c-myc (D84C12, Cell Signaling), and *β*-tubulin (sc-55529, Santa Cruz Biotechnology, Inc) were incubated with the membranes overnight at 4 °C. respectively. IRDye 680LT goat anti-mouse IgG (827-11080, LiCOR) or IRDye 800CW goat anti-rabbit IgG (827-08365, LiCOR) was used as the secondary antibody. The images were detected by the Odyssey Infrared Imaging System (LiCOR). Experiments were performed in duplicate.

Co-IP assays. Two sets of co-IP experiments were conducted: one is the inhibitor was added onto the cell lysates, and the second is the inhibitor was added onto the live cells. For the cell lysate co-IP experiments, HCT116 cells were lysed first in buffer A containing 50 mM Tris, pH 7.4, 150 mM NaCl, 1% Nonidet P-40, 2 mM EDTA, and protease inhibitors. Different concentrations of the inhibitor were incubated with the HCT116 cell lysates at 4 °C for 4 h. For the whole cell co-IP experiments, HCT116 cells at 1×10^6/mL were treated with different concentrations of the inhibitor for 24 h. Cells were then lysed in buffer containing 50 mM Tris, pH 7.4, 150 mM NaCl, 1% Nonidet P-40, 2 mM EDTA, and protease inhibitors. For both cell lysate and whole cell co-IP experiments, the lysates were then preadsorbed to A/G plus agarose (sc-2003, Santa Cruz Biotechnology) at 4 °C for 1 h. Preadsorbed lysates were incubated with a specific primary antibody against *β*-catenin (610153, BD Biosciences) overnight at 4 °C. A/G plus agarose was then added to the lysate mixture and incubated for 3 h. The beads were washed 5 times with the lysis buffer at 4 °C. The bound protein was eluted by boiling in the SDS sample buffer and loaded

onto 8% SDS polyacrylamide gel for electrophoretic analysis. Separated proteins were transferred onto nitrocellulose membranes for immunoblot analysis. The antibodies against BCL9 (ab37305, Abcam) and E-cadherin (610404, BD Biosciences) were incubated with the membranes, respectively. IRDye 680LT goat anti-mouse IgG (827-11080, LiCOR) was used as the secondary antibody. The images were detected by the Odyssey Infrared Imaging System (LiCOR). Experiments were performed in duplicate.

ASSOCIATED CONTENT

Supporting Information

The supporting information is available free of charge on the ACS Publications website at DOI: 10.1021/

The determination of the intracellular concentration of **29**, the description of the hot region 2 for the *β*-catenin/BCL9 PPI, the stick models of AutoDock docking results of **3** and **29** with *β*-catenin, the LDH cytotoxicity assay results of **1**–**9** and **11**–**31**, The quantitative data for Western blot and co-IP experiments, the synthesis and structural characterizations of **4**–**26**, the HPLC conditions and traces, and NMR spectra of **2**–**32**, and molecular formula strings.

AUTHOR INFORMATION

Corresponding Author

* H.J.: Phone, (813) 745-8070; Fax, (813) 745-4506; E-mail: Haitao.Ji@moffitt.org

ORCID

Haitao Ji: 0000-0001-5526-4503

Notes

The authors declare no competing financial interest.

ACKNOWLEDGMENTS

This work was supported by the Department of Defense CDMRP BCRP breakthrough award W81XWH-14-1-0083. We thank John A. Wisniewski, Daniel Powell, and Jinya Yin for the initial synthesis of some compounds. The H. Lee Moffitt Cancer Center & Research Institute is a NCI-designated Comprehensive Cancer Center, supported under NIH grant P30-CA76292.

ABBREVIATIONS USED

ABC, the active form of β-catenin; APC, adenomatous polyposis coli; BCL9, B-cell lymphoma 9; B9L, BCL9-like; CBP, CREB-binding protein; co-IP, co-immunoprecipitation; DAD, diode array detector; DPPA, diphenylphosphoryl azide; Dvl, disheveled; Fzd, frizzled; HD2, homology domain 2; K_D, dissociation constant; LDH, lactate dehydrogenase; Lef, lymphoid enhancer-binding factor; LRP5/6, low-density lipoprotein-related proteins 5 and 6; PMS, phenazine methosulfat; PPI, protein–protein interaction; qPCR, quantitative real-time PCR; sFRP1, secreted Fzd-related protein 1; Tcf, T-cell factor.

REFERENCES

1. Nusse, R.; Clevers, H. Wnt/*β*-catenin signaling, disease, and emerging therapeutic modalities. *Cell* **2017**, *169*, 985–999.
2. Anastas, J. N.; Moon, R. T. WNT signalling pathways as therapeutic targets in cancer. *Nat. Rev. Cancer*. **2013**, *13*, 11–26.
3. van de Wetering, M.; Sancho, E.; Verweij, C.; de Lau, W.; Oving, I.; Hurlstone, A.; van der Horn, K.; Batlle, E.; Coudreuse, D.; Haramis, A.-P.; Tjon-Pon-Fong, M.; Moerer, P.; van den Born, M.; Soete, G.; Pals, S.; Eilers, M.; Medema, R.; Clevers, H. The *β*-catenin/TCF-4 complex imposes a crypt progenitor phenotype on colorectal cancer cells. *Cell* **2002**, *111*, 241–250.
4. Lu, D.; Zhao, Y.; Tawatao, R.; Cottam, H. B.; Sen, M.; Leoni, L. M.; Kipps, T. J.; Corr, M.; Carson, D. A. Activation of the Wnt signaling pathway in chronic lymphocytic leukemia. *Proc. Natl. Acad. Sci. U.S.A.* **2004**, *101*, 3118–3123.
5. Sukhdeo, K.; Mani, M.; Zhang, Y.; Dutta, J.; Yasui, H.; Rooney, M. D.; Carrasco, D. E.; Zheng, M.; He, H.; Tai, Y.-T.; Mitsiades, C.; Anderson, K. C.; Carrasco, D. R. Targeting the *β*-catenin/TCF transcriptional complex in the treatment of multiple myeloma. *Proc. Natl. Acad. Sci. U.S.A.* **2007**, *104*, 7516–7521.
6. Dow, L. E.; O'Rourke, K. P.; Simon, J.; Tschaharganeh, D. F.; van Es, J. H.; Clevers, H.; Lowe, S. W. Apc restoration promotes cellular differentiation and reestablishes crypt homeostasis in colorectal cancer. *Cell* **2015**, *161*, 1539–1552.
7. Brack, A. S.; Conboy, M. J.; Roy, S.; Lee, M.; Kuo, C. J.; Keller, C.; Rando, T. A. Increased Wnt signaling during aging alters muscle stem cell fate and increases fibrosis. *Science* **2007**, *317*, 807–810.

8. Lancaster, M. A.; Louie, C. M.; Silhavy, J. L.; Sintasath, L.; Decambre, M.; Nigam, S. K.; Willert, K.; Gleeson, J. G. Impaired Wnt-*β*-catenin signaling disrupts adult renal homeostasis and leads to cystic kidney ciliopathy. *Nat. Med.* **2009**, *15*, 1046–1054.

9. Akhmetshina, A.; Palumbo, K.; Dees, C.; Bergmann, C.; Venalis, P.; Zerr, P.; Horn, A.; Kireva, T.; Beyer, C.; Zwerina, J.; Schneider, H.; Sadowski, A.; Riener, M.-O.; MacDougald, O. A.; Distler, O.; Schett, G.; Distler, J. H. W. Activation of canonical Wnt signalling is required for TGF-*β*-mediated fibrosis. *Nat. Commun.* **2012**, *3*, 735.

10. Malanchi, I.; Peinado, H.; Kassen, D.; Hussenet, T.; Metzger, D.; Chambon, P.; Huber, M.; Hohl, D.; Cano, A.; Birchmeier, W.; Huelsken, J. Cutaneous cancer stem cell maintenance is dependent on *β*-catenin signalling. *Nature* **2008**, *452*, 650–653.

11. Barker, N.; Ridgway, R. A.; van Es, J. H.; van de Wetering, M.; Begthel, H.; van den Born, M.; Danenberg, E.; Clarke, A. R.; Sansom, O. J.; Clevers, H. Crypt stem cells as the cells-of-origin of intestinal cancer. *Nature* **2009**, *457*, 608–611.

12. Wang, Y.; Krivtsov, A. V.; Sinha, A. U.; North, T. E.; Goessling, W.; Feng, Z.; Zon, L. I.; Armstrong, S. A. The Wnt/*β*-catenin pathway is required for the development of leukemia stem cells in AML. *Science* **2010**, *327*, 1650–1653.

13. Huebschman, M. L.; Lane, N. L.; Liu, H.; Sarode, V. R.; Devlin, J. L.; Frenkel, E. P. Molecular heterogeneity in adjacent cells in triple-negative breast cancer. *Breast Cancer* **2015**, *7*, 231–237.

14. Tammela, T.; Sanchez-Rivera, F. J.; Cetinbas, N. M.; Wu, K.; Joshi, N. S.; Helenius, K.; Park, Y.; Azimi, R.; Kerper, N. R.; Wesselhoeft, R. A.; Gu, X.; Schmidt, L.; Cornwall-Brady, M.; Yilmaz, Ö. H.; Xue, W.; Katajisto, P.; Bhutkar, A.; Jacks, T. A Wnt-producing

niche drives proliferative potential and progression in lung adenocarcinoma. *Nature* **2017**, *545*, 355–359.

15. Malanchi, I.; Santamaria-Martínez, A.; Susanto, E.; Peng, H.; Lehr, H.-A.; Delaloye, J.-F.; Huelsken, J. Interactions between cancer stem cells and their niche govern metastatic colonization. *Nature* **2011**, *481*, 85–89.
16. Creighton, C. J.; Li, X.; Landis, M.; Dixon, J. M.; Neumeister, V. M.; Sjolund, A.; Rimm, D. L.; Wong, H.; Rodriguez, A.; Herschkowitz, J. I.; Fan, C.; Zhang, X.; He, X.; Pavlick, A.; Gutierrez, M. C.; Renshaw, L.; Larionov, A. A.; Faratian, D.; Hilsenbeck, S. G.; Perou, C. M.; Lewis, M. T.; Rosen, J. M.; Chang, J. C. Residual breast cancers after conventional therapy display mesenchymal as well as tumor-initiating features. *Proc. Natl. Acad. Sci. U.S.A.* **2009**, *106*, 13820–13825.
17. Yeung, J.; Esposito, M. T.; Gandillet, A.; Zeisig, B. B.; Griessinger, E.; Bonnet, D.; So, C. W. E. *β*-Catenin mediates the establishment and drug resistance of MLL leukemic stem cells. *Cancer Cell* **2010**, *18*, 606–618.
18. Fong, C. Y.; Gilan, O.; Lam, E. Y. N.; Rubin, A. F.; Ftouni, S.; Tyler, D.; Stanley, K.; Sinha, D.; Yeh, P.; Morison, J.; Giotopoulos, G.; Lugo, D.; Jeffrey, P.; Lee, S. C.-W.; Carpenter, C.; Gregory, R.; Ramsay, R. G.; Lane, S. W.; Abdel-Wahab, O.; Kouzarides, T.; Johnstone, R. W.; Dawson, S.-J.; Huntly, B. J. P.; Prinjha, R. K.; Papenfuss, A. T.; Dawson, M. A. BET inhibitor resistance emerges from leukaemia stem cells. *Nature* **2015**, *525*, 538–542.
19. Milanovic, M.; Fan, D. N. Y.; Belenki, D.; Däbritz, J. H. M.; Zhao, Z.; Yu, Y.; Dörr, J. R.; Dimitrova, L.; Lenze, D.; Monteiro Barbosa, I. A.; Mendoza-Parra, M. A.; Kanashova, T.; Metzner, M.; Pardon, K.; Reimann, M.; Trumpp, A.; Dörken, B.; Zuber, J.; Gronemeyer,

H.; Hummel, M.; Dittmar, G.; Lee, S.; Schmitt, C. A. Senescence-associated reprogramming promotes cancer stemness. *Nature* **2018**, *553*, 96–100.

20. Spranger, S.; Bao, R.; Gajewski, T. F. Melanoma-intrinsic *β*-catenin signalling prevents anti-tumour immunity. *Nature* **2015**, *523*, 231–235.
21. Sweis, R. F.; Spranger, S.; Bao, R.; Paner, G. P.; Stadler, W. M.; Steinberg, G.; Gajewski, T. F. Molecular drivers of the non-T-cell-inflamed tumor microenvironment in urothelial bladder cancer. *Cancer Immunol. Res.* **2016**, *4*, 563–568.
22. Ding, Y.; Shen, S.; Lino, A. C.; Curotto de Lafaille, M. A.; Lafaille, J. J. *β*-Catenin stabilization extends regulatory T cell survival and induces anergy in nonregulatory T cells. *Nat. Med.* **2008**, *14*, 162–169.
23. Keerthivasan, S.; Aghajani, K.; Dose, M.; Molinero, L.; Khan, M. W.; Venkateswaran, V.; Weber, C.; Emmanuel, A. O.; Sun, T.; Bentrem, D. J.; Mulcahy, M.; Keshavarzian, A.; Ramos, E. M.; Blatner, N.; Khazaie, K.; Gounari, F. *β*-Catenin promotes colitis and colon cancer through imprinting of proinflammatory properties in T cells. *Sci. Transl. Med.* **2014**, *6*, 225ra28.
24. Chen, B.; Dodge, M. E.; Tang, W.; Lu, J.; Ma, Z.; Fan, C.-W.; Wei, S.; Hao, W.; Kilgore, J.; Williams, N. S.; Roth, M. G.; Amatruda, J. F.; Chen, C.; Lum, L. Small molecule-mediated disruption of Wnt-dependent signaling in tissue regeneration and cancer. *Nat. Chem. Biol.* **2009**, *5*, 100–107.
25. Proffitt, K. D.; Madan, B.; Ke, Z.; Pendharkar, V.; Ding, L.; Lee, M. A.; Hannoush, R. N.; Virshup, D. M. Pharmacological inhibition of the Wnt acyltransferase PORCN prevents growth of WNT-driven mammary cancer. *Cancer Res.* **2013**, *73*, 502–507.

26. Lum, L.; Clevers, H. Cell biology. The unusual case of Porcupine. *Science* **2012**, *337*, 922–923.

27. Lu, D.; Choi, M. Y.; Yu, J.; Castro, J. E.; Kipps, T. J.; Carson, D. A. Salinomycin inhibits Wnt signaling and selectively induces apoptosis in chronic lymphocytic leukemia cells. *Proc. Natl. Acad. Sci. U.S.A.* **2011**, *108*, 13253–13257.

28. Fujii, N.; You, L.; Xu, Z.; Uematsu, K.; Shan, J.; He, B.; Mikami, I.; Edmondson, L. R.; Neale, G.; Zheng, J.; Guy, R. K.; Jablons, D. M. An antagonist of dishevelled protein-protein interaction suppresses β-catenin-dependent tumor cell growth. *Cancer Res.* **2007**, *67*, 573–579.

29. Thorne, C. A.; Hanson, A. J.; Schneider, J.; Tahinci, E.; Orton, D.; Cselenyi, C. S.; Jernigan, K. K.; Meyers, K. C.; Hang, B. I.; Waterson, A. G.; Kim, K.; Melancon, B.; Ghidu, V. P.; Sulikowski, G. A.; LaFleur, B.; Salic, A.; Lee, L. A.; Miller, D. M. III.; Lee, E. Small-molecule inhibition of Wnt signaling through activation of casein kinase 1α. *Nat Chem. Biol.* **2010**, *6*, 829–836.

30. Huang, S.-M.; Mishina, Y. M.; Liu, S.; Cheung, A.; Stegmeier, F.; Michaud, G. A.; Charlat, O.; Wiellette, E.; Zhang, Y.; Wiessner, S.; Hild, M.; Shi, X.; Wilson, C. J.; Mickanin, C.; Myer, V.; Fazal, A.; Tomlinson, R.; Serluca, F.; Shao, W.; Cheng, H.; Shultz, M.; Rau, C.; Schirle, M.; Schlegl, J.; Ghidelli, S.; Fawell, S.; Lu, C.; Curtis, D.; Kirschner, M. W.; Lengauer, C.; Finan, P. M.; Tallarico, J. A.; Bouwmeester, T.; Porter, J. A.; Bauer, A.; Cong, F. Tankyrase inhibition stabilizes axin and antagonizes Wnt signalling. *Nature* **2009**, *461*, 614–620.

31. Waaler, J.; Machon, O.; Tumova, L.; Dinh, H.; Korinek, V.; Wilson, S. R.; Paulsen, J. E.; Pedersen, N. M.; Eide, T. J.; Machonova, O.; Gradl, D.; Voronkov, A.; von Kries, J. P.;

Krauss, S. A novel tankyrase inhibitor decreases canonical Wnt signaling in colon carcinoma cells and reduces tumor growth in conditional APC mutant mice. *Cancer Res.* **2012**, *72*, 2822–2832.

32. Kramps, T.; Peter, O.; Brunner, E.; Nellen, D.; Froesch, B.; Chatterjee, S.; Murone, M.; Züllig, S.; Basler, K. Wnt/wingless signaling requires BCL9/legless-mediated recruitment of pygopus to the nuclear *β*-catenin-TCF complex. *Cell* **2002**, *109*, 47–60.
33. van Tienen, L. M.; Mieszczanek, J.; Fiedler, M.; Rutherford, T. J.; Bienz, M. Constitutive scaffolding of multiple Wnt enhanceosome components by Legless/BCL9. *Elife* **2017**, *6*, e20882.
34. Sampietro, J.; Dahlberg, C. L.; Cho, U. S.; Hinds, T. R.; Kimelman, D.; Xu, W. Crystal structure of a *β*-catenin/BCL9/Tcf4 complex. *Mol. Cell.* **2006**, *24*, 293–300.
35. de la Roche, M.; Rutherford, T. J.; Gupta, D.; Veprintsev, D. B.; Saxty, B.; Freund, S. M.; Bienz, M. An intrinsically labile α-helix abutting the BCL9-binding site of *β*-catenin is required for its inhibition by carnosic acid. *Nat. Commun.* **2012**, *3*, 680.
36. Hoffmans, R.; Basler, K. Identification and *in vivo* role of the Armadillo-Legless interaction. *Development* **2004**, *131*, 4393–4400.
37. Hoffmans. R.; Basler, K. BCL9-2 binds Arm/*β*-catenin in a Tyr142-independent manner and requires Pygopus for its function in Wg/Wnt signaling. *Mech. Dev.* **2007**, *124*, 59–67.
38. Valenta, T.; Gay, M.; Steiner, S.; Draganova, K.; Zemke, M.; Hoffmans, R.; Cinelli, P.; Aguet, M.; Sommer, L.; Basler, K. Probing transcription-specific outputs of *β*-catenin *in vivo*. *Genes Dev.* **2011**, *25*, 2631–2643.
39. Adachi, S.; Jigami, T.; Yasui, T.; Nakano, T.; Ohwada, S.; Omori, Y.; Sugano, S.; Ohkawara, B.; Shibuya, H.; Nakamura, T.; Akiyama, T. Role of a BCL9-related *β*-catenin-

binding protein, B9L, in tumorigenesis induced by aberrant activation of Wnt signaling. *Cancer Res.* **2004**, *64*, 8496–8501.

40. Brembeck, F. H.; Schwarz-Romond, T.; Bakkers, J.; Wilhelm, S.; Hammerschmidt, M.; Birchmeier, W. Essential role of BCL9-2 in the switch between *β*-catenin's adhesive and transcriptional functions. *Genes Dev.* **2004**, *18*, 2225–2230.
41. de la Roche, M.; Worm, J.; Bienz, M. The function of BCL9 in Wnt/*β*-catenin signaling and colorectal cancer cells. *BMC Cancer* **2008**, *8*, 199.
42. Brembeck, F. H.; Wiese, M.; Zatula, N.; Grigoryan, T.; Dai, Y.; Fritzmann, J.; Birchmeier, W. BCL9-2 promotes early stages of intestinal tumor progression. *Gastroenterology* **2011**, *141*, 1359–1370.
43. Mani, M.; Carrasco, D. E.; Zhang, Y.; Takada, K.; Gatt, M. E.; Dutta-Simmons, J.; Ikeda, H.; Diaz-Griffero, F.; Pena-Cruz, V.; Bertagnolli, M.; Myeroff, L. L.; Markowitz, S. D.; Anderson, K. C.; Carrasco, D. R. BCL9 promotes tumor progression by conferring enhanced proliferative, metastatic, and angiogenic properties to cancer cells. *Cancer Res.* **2009**, *69*, 7577–7586.
44. Kawamoto, S. A.; Coleska, A.; Ran, X.; Yi, H.; Yang, C.-Y.; Wang, S. Design of triazole-stapled BCL9 α-helical peptides to target the *β*-catenin/B-cell CLL/lymphoma 9 (BCL9) protein-protein interaction. *J. Med. Chem.* **2012**, *55*, 1137–1146.
45. Takada, K.; Zhu, D.; Bird, G. H.; Sukhdeo, K.; Zhao, J.-J.; Mani, M.; Lemieux, M.; Carrasco, D. E.; Ryan, J.; Horst, D.; Fulciniti, M.; Munshi, N. C.; Xu, W.; Kung, A. L.; Shivdasani, R. A.; Walensky, L. D.; Carrasco, D. R. Targeted disruption of the BCL9/*β*-catenin complex inhibits oncogenic Wnt signaling. *Sci. Transl. Med.* **2012**, *4*, 148ra117.

46. de la Roche, M.; Ibrahim, A. E.; Mieszczanek, J.; Bienz, M. LEF1 and B9L shield *β*-catenin from inactivation by Axin, desensitizing colorectal cancer cells to tankyrase inhibitors. *Cancer Res.* **2014**, *74*, 1495–1505.

47. Hoggard, L. R.; Zhang, Y.; Zhang, M.; Panic, V.; Wisniewski, J. A.; Ji, H. Rational design of selective small-molecule inhibitors for *β*-catenin/B-cell lymphoma 9 protein-protein interactions. *J. Am. Chem. Soc.* **2015**, *137*, 12249–12260.

48. Teuscher, K. B.; Zhang, M.; Ji, H. A versatile method to determine the cellular bioavailability of small-molecule inhibitors. *J. Med. Chem.* **2017**, *60*, 157–169.

49. Kawamoto, S. A.; Thompson, A. D.; Coleska, A.; Nikolovska-Coleska, Z.; Yi, H.; Wang, S. Analysis of the interaction of BCL9 with *β*-catenin and development of fluorescence polarization and surface plasmon resonance binding assays for this interaction. *Biochemistry* **2009**, *48*, 9534–9541.

50. Zhang, M.; Wisniewski, J. A.; Ji, H AlphaScreen selectivity assay for *β*-catenin/B-cell lymphoma 9 inhibitors. *Anal. Biochem.* **2015**, *469*, 43–53.

51. Pennington, L. D.; Moustakas, D. T. The necessary nitrogen atom: a versatile high-impact design element for multiparameter optimization. *J. Med. Chem.* **2017**, *60*, 3552–3579.

52. Huber, A. H.; Weis, W. I. The structure of the *β*-catenin/E-cadherin complex and the molecular basis of diverse ligand recognition by *β*-catenin. *Cell* **2001**, *105*, 391–402.

53. Barltrop, J. A.; Owen, T. C.; Cory, A. H.; Cory, J. G. 5-(3-Carboxymethoxyphenyl)-2-(4,5-dimethylthiazolyl)-3-(4-sulfophenyl) tetrazolium, inner salt (MTS) and related analogs of 3-(4,5-dimethylthiazolyl)-2,5-diphenyltetrazolium bromide (MTT) reducing to purple water-soluble formazans as cell-viability indicators. *Bioorg. Med. Chem. Lett.* **1991**, *1*, 611–614.

54. Cory, A. H.; Owen, T. C.; Barltrop, J. A.; Cory, J. G. Use of an aqueous soluble tetrazolium/formazan assay for cell growth assays in culture. *Cancer Commun.* **1991**, *3*, 207–212.

55. Nachlas, M. M.; Margulies, S. I.; Goldberg, J. D.; Seligman, A. M. The determination of lactic dehydrogenase with a tetrazolium salt. *Anal. Biochem.* **1960**, *1*, 317–326.

56. Decker, T.; Lohmann-Matthes, M. -L. A quick and simple method for the quantitation of lactate dehydrogenase release in measurements of cellular cytotoxicity and tumor necrosis factor (TNF) activity. *J. Immunol. Methods* **1988**, *115*, 61–69.

57. Niles, A. L.; Moravec, R. A.; Riss, T. L. *In vitro* viability and cytotoxicity testing and same-well multi-parametric combinations for high throughput screening. *Curr. Chem. Genomics* **2009**, *3*, 33–41.

58. Yan, D.; Wiesmann, M.; Rohan, M.; Chan, V.; Jefferson, A. B.; Guo, L.; Sakamoto, D.; Caothien, R. H.; Fuller, J. H.; Reinhard, C.; Garcia, P. D.; Randazzo, F. M.; Escobedo, J.; Fantl, W. J.; Williams, L. T. Elevated expression of *axin2* and *hnkd* mRNA provides evidence that Wnt/*β*-catenin signaling is activated in human colon tumors. *Proc. Natl. Acad. Sci. U.S.A.* **2001**, *98*, 14973–14978.

59. Wisniewski, J. A.; Yin, J.; Teuscher, K. B.; Zhang, M.; Ji, H. Structure-based design of 1,4-dibenzoylpiperazines as *β*-catenin/B-cell lymphoma 9 protein–protein interaction inhibitors. *ACS Med. Chem. Lett.* **2016**, *7*, 508–513.

60. Ji, X.; Huang, H.; Li, Y.; Chen, H.; Jiang, H. Palladium-catalyzed sequential formation of C–C bonds: efficient assembly of 2-substituted and 2,3-disubstituted quinolones. *Angew. Chem. Int. Ed.* **2012**, *51*, 7292–7296.

61. Zhang, Y.; Wang, M.; Li, P.; Wang, L. Iron-promoted tandem reaction of anilines with styrene oxides via C-C cleavage for the synthesis of quinolines. *Org. Lett.* **2012**, *14*, 2206–2209.

62. Kahn, M. Can we safely target the WNT pathway? *Nature Rev. Drug Discov.* **2014**, *13*, 513–532.

63. Emami, K. H.; Nguyen, C.; Ma, H.; Kim, D. H.; Jeong, K. W.; Eguchi, M.; Moon, R. T.; Teo, J.-L.; Kim, H. Y.; Moon, S. H.; Ha, J. R.; Kahn, M. A small molecule inhibitor of *β*-catenin/CREB-binding protein transcription. *Proc. Natl. Acad. Sci. U.S.A.* **2004**, *101*, 12682-12687.

64. Kimura, K.; Ikoma, A.; Shibakawa, M.; Shimoda, S.; Harada, K.; Saio, M.; Imamura, J.; Osawa, Y.; Kimura, M.; Nishikawa, K.; Okusaka, T.; Morita, S.; Inoue, K.; Kanto, T.; Todaka, K.; Nakanishi, Y.; Kohara, M.; Mizokami, M. Safety, tolerability, and preliminary efficacy of the anti-fibrotic small molecule PRI-724, a CBP/*β*-catenin inhibitor, in patients with hepatitis C virus-related cirrhosis: a single-center, open-label, dose escalation phase 1 trial. *EBioMedicine* **2017**, *23*, 79–87.

65. Kim, Y.-M.; Ma, H.; Oehler, V. G.; Gang, E. J.; Nguyen, C.; Masiello, D.; Liu, H.; Zhao, Y.; Radich, J.; Kahn, M. The *γ*-catenin/CBP complex maintains survivin transcription in *β*-catenin deficient/depleted cancer cells. *Curr. Cancer Drug Targets* **2011**, *11*, 213–225.

66. Townsley, F. M.; Thompson, B.; Bienz, M. Pygopus residues required for its binding to Legless are critical for transcription and development. *J. Biol. Chem.* **2004**, *279*, 5177–5183.

67. Thompson, B. J. A complex of Armadillo, Legless, and Pygopus coactivates dTCF to activate wingless target genes. *Curr. Biol.* **2004**, *14*, 458–466.

68. Townsley, F. M.; Cliffe, A.; Bienz, M. Pygopus and Legless target Armadillo/*β*-catenin to the nucleus to enable its transcriptional co-activator function. *Nat. Cell Biol.* **2004**, *6*, 626–633.

69. Hoffmans, R.; Städeli, R.; Basler, K. Pygopus and legless provide essential transcriptional coactivator functions to armadillo/*β*-catenin. *Curr. Biol.* **2005**, *15*, 1207–1211.

70. Sakamoto, I.; Ohwada, S.; Toya, H.; Togo, N.; Kashiwabara, K.; Oyama, T.; Nakajima, T.; Ito, H.; Adachi, S.; Jigami, T.; Akiyama, T. Up-regulation of a BCL9-related *β*-catenin-binding protein, B9L, in different stages of sporadic colorectal adenoma. *Cancer Sci.* **2007**, *98*, 83–87.

71. Deka, J.; Wiedemann, N.; Anderle, P.; Murphy-Seiler, F.; Bultinck, J.; Eyckerman, S.; Stehle, J.-C.; André, S.; Vilain, N.; Zilian, O.; Robine, S.; Delorenzi, M.; Basler, K.; Aguet, M. Bcl9/Bcl9l are critical for Wnt-mediated regulation of stem cell traits in colon epithelium and adenocarcinomas. *Cancer Res.* **2010**, *70*, 6619–6628.

72. Moor, A. E.; Anderle, P.; Cantù, C.; Rodriguez, P.; Wiedemann, N.; Baruthio, F.; Deka, J.; André, S.; Valenta, T.; Moor, M. B.; Győrffy, B.; Barras, D.; Delorenzi, M.; Basler, K.; Aguet, M. BCL9/9L-*β*-catenin signaling is associated with poor outcome in colorectal cancer. *EBioMedicine* **2015**, *2*, 1932–1943.

73. Leeson, P. D.; Springthorpe, B. The influence of drug-like concepts on decision-making in medicinal chemistry. *Nat. Rev. Drug Discov.* **2007**, *6*, 881–890.

74. Azzaoui, K.; Hamon, J.; Faller, B.; Whitebread, S.; Jacoby, E.; Bender, A.; Jenkins, J. L.; Urban, L. Modeling promiscuity based on *in vitro* safety pharmacology profiling data. *ChemMedChem* **2007**, *2*, 874–880.

75. Peters, J.-U.; Schnider, P.; Mattei, P.; Kansy, M. Pharmacological promiscuity: dependence on compound properties and target specificity in a set of recent Roche compounds. *ChemMedChem* **2009**, *4*, 680–686.

76. Peters, J.-U.; Hert, J.; Bissantz, C.; Hillebrecht, A.; Gerebtzoff, G.; Bendels, S.; Tillier, F.; Migeon, J.; Fischer, H.; Guba, W.; Kansy, M. Can we discover pharmacological promiscuity early in the drug discovery process? *Drug Discov. Today* **2012**, *17*, 325–335.

77. Nishisho, I.; Nakamura, Y.; Miyoshi, Y.; Miki, Y.; Ando, H.; Horii, A.; Koyama, K.; Utsunomiya, J.; Baba, S.; Hedge, P. Mutations of chromosome 5q21 genes in FAP and colorectal cancer patients. *Science* **1991**, *253*, 665–669.

78. Ilyas, M.; Tomlinson, I. P. M.; Rowan, A.; Pignatelli, M.; Bodmer, W. F. *β*-Catenin mutations in cell lines established from human colorectal cancers. *Proc. Natl. Acad. Sci. U.S.A.* **1997**, *94*, 10330–10334.

79. Bilir, B.; Kucuk, O.; Moreno, C. S. Wnt signaling blockage inhibits cell proliferation and migration, and induces apoptosis in triple-negative breast cancer cells. *J. Transl. Med.* **2013**, *11*, 280.

80. Xu, J.; Prosperi, J. R.; Choudhury, N.; Olopade, O. I.; Goss, K. H. *β*-Catenin is required for the tumorigenic behavior of triple-negative breast cancer cells. *PLoS One* **2015**, *10*, e0117097.

81. Maubant, S.; Tesson, B.; Maire, V.; Ye, M.; Rigaill, G.; Gentien, D.; Cruzalegui, F.; Tucker, G. C.; Roman-Roman, S.; Dubois, T. Transcriptome analysis of Wnt3a-treated triple-negative breast cancer cells. *PLoS One* **2015**, *10*, e0122333.

82. Liu, C.-C.; Prior, J.; Piwnica-Worms, D.; Bu, G. LRP6 overexpression defines a class of breast cancer subtype and is a target for therapy. *Proc. Natl. Acad. Sci. U.S.A.* **2010**, *107*, 5136–5141.

83. Yang, L.; Wu, X.; Wang, Y.; Zhang, K.; Wu, J.; Yuan, Y.-C.; Deng, X.; Chen, L.; Kim, C. C. H.; Lau, S.; Somlo, G.; Yen, Y. FZD7 has a critical role in cell proliferation in triple negative breast cancer. *Oncogene* **2011**, *30*, 4437–4446.

84. Corda, G.; Sala, G.; Lattanzio, R.; Iezzi, M.; Sallese, M.; Fragassi, G.; Lamolinara, A.; Mirza, H.; Barcaroli, D.; Ermler, S.; Silva, E.; Yasaei, H.; Newbold, R. F.; Vagnarelli, P.; Mottolese, M.; Natali, P. G.; Perracchio, L.; Quist, J.; Grigoriadis, A.; Marra, P.; Tutt, A. N.; Piantelli, M.; Iacobelli, S.; De Laurenzi, V.; Sala, A. Functional and prognostic significance of the genomic amplification of frizzled 6 (FZD6) in breast cancer. *J. Pathol.* **2017**, *241*, 350–361.

85. Wend, P.; Runke, S.; Wend, K.; Anchondo, B.; Yesayan, M.; Jardon, M.; Hardie, N.; Loddenkemper, C.; Ulasov, I.; Lesniak, M. S.; Wolsky, R.; Bentolila, L. A.; Grant, S. G.; Elashoff, D.; Lehr, S.; Latimer, J. J.; Bose, S.; Sattar, H.; Krum, S. A.; Miranda-Carboni, G. A. WNT10B/*β*-catenin signalling induces HMGA2 and proliferation in metastatic triple-negative breast cancer. *EMBO Mol. Med.* **2013**, *5*, 264–279.

86. Dey, N.; Barwick, B. G.; Moreno, C. S.; Ordanic-Kodani, M.; Chen, Z.; Oprea-Ilies, G.; Tang, W.; Catzavelos, C.; Kerstann, K. F.; Sledge, G. W. Jr.; Abramovitz, M.; Bouzyk, M.; De, P.; Leyland-Jones, B. R. Wnt signaling in triple negative breast cancer is associated with metastasis. *BMC Cancer* **2013**, *13*, 537.

87. Uematsu, K.; He, B.; You, L.; Xu, Z.; McCormick, F.; Jablons, D. M. Activation of the Wnt pathway in non small cell lung cancer: evidence of dishevelled overexpression. *Oncogene* **2003**, *22*, 7218–7221.

88. Grossmann, T. N.; Yeh, J. T.-H.; Bowman, B. R.; Chu, Q.; Moellering, R. E.; Verdine, G. L. Inhibition of oncogenic Wnt signaling through direct targeting of *β*-catenin. *Proc. Natl. Acad. Sci. U.S.A.* **2012**, *109*, 17942–17947.

89. Ritchie, T. J.; Macdonald, S. J. F. The impact of aromatic ring count on compound developability--are too many aromatic rings a liability in drug design? *Drug Discov. Today* **2009**, *14*, 1011–1020.

90. Ritchie, T. J.; Macdonald, S. J. F.; Young, R. J.; Pickett, S. D. The impact of aromatic ring count on compound developability: further insights by examining carbo- and hetero-aromatic and -aliphatic ring types. *Drug Discov. Today* **2011**, *16*, 164–171.

91. Young, R. J.; Green, D. V. S.; Luscombe, C. N.; Hill, A. P. Getting physical in drug discovery II: the impact of chromatographic hydrophobicity measurements and aromaticity. *Drug Discov. Today* **2011**, *16*, 822–830.

92. Ritchie, T. J.; Macdonald, S. J. F. Physicochemical descriptors of aromatic character and their use in drug discovery. *J. Med. Chem.* **2014**, *57*, 7206–7215.

93. Nikolovska-Coleska, Z.; Wang, R.; Fang, X.; Pan, H.; Tomita, Y.; Li, P.; Roller, P. P.; Krajewski, K.; Saito, N. G.; Stuckey, J. A.; Wang, S. Development and optimization of a binding assay for the XIAP BIR3 domain using fluorescence polarization. *Anal. Biochem.* **2004**, *332*, 261–273.

Table of Contents Graphic